

\mathcal{PT} symmetry breaking and exceptional points for a class of inhomogeneous complex potentials

Patrick Dorey¹, Clare Dunning², Anna Lishman³ and Roberto Tateo⁴

^{1,3}*Dept. of Mathematical Sciences, University of Durham, Durham DH1 3LE, UK*

²*IMSAS, University of Kent, Canterbury, UK CT2 7NF, United Kingdom*

⁴*Dip. di Fisica Teorica and INFN, Università di Torino,
Via P. Giuria 1, 10125 Torino, Italy*

Abstract

We study a three-parameter family of \mathcal{PT} -symmetric Hamiltonians, related via the ODE/IM correspondence to the Perk-Schultz models. We show that real eigenvalues merge and become complex at quadratic and cubic exceptional points, and explore the corresponding Jordan block structures by exploiting the quasi-exact solvability of a subset of the models. The mapping of the phase diagram is completed using a combination of numerical, analytical and perturbative approaches. Among other things this reveals some novel properties of the Bender-Dunne polynomials, and gives a new insight into a phase transition to infinitely-many complex eigenvalues that was first observed by Bender and Boettcher. A new exactly-solvable limit, the inhomogeneous complex square well, is also identified.

¹p.e.dorey@durham.ac.uk

²t.c.dunning@kent.ac.uk

³AnnaLishman@dunelm.org.uk

⁴tateo@to.infn.it

1 Introduction

In this paper we return to the spectra of a family of \mathcal{PT} -symmetric eigenvalue problems first studied in detail in [1,2]. Consider the following differential operator:

$$\mathcal{H} = -\frac{d^2}{dx^2} - (ix)^{2M} - \alpha(ix)^{M-1} + \frac{\lambda^2 - \frac{1}{4}}{x^2}, \quad (1.1)$$

where M , α and λ are real numbers, with $M > 0$, and the powers of ix are rendered single-valued by placing a cut along the positive imaginary x axis. Then an eigenvalue problem, with a discrete spectrum, can be defined as

$$\mathcal{H}\psi(x) = E\psi(x); \quad \psi(x) \in L^2(\mathcal{C}), \quad (1.2)$$

where \mathcal{C} is an infinite contour in the complex plane, which must pass below the origin whenever $\lambda^2 \neq \frac{1}{4}$ or $M \notin \mathbb{Z}$. For $M < 2$ the ends of this contour can asymptote to the negative and positive real axes, while for $M \geq 2$ they must be deformed down into the complex plane so as to continue the $M < 2$ spectral problem smoothly [3]. This is illustrated in figure 1.

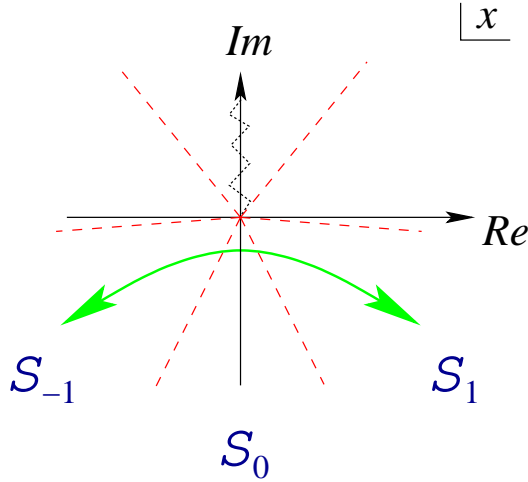


Figure 1: A possible quantisation contour \mathcal{C} for M just larger than 2, together with some of the Stokes sectors.

In [1, 2], the eigenvalue problem was initially specified in terms of $l \equiv \lambda - \frac{1}{2}$, but with boundary conditions imposed at infinity, the choice of λ is more natural.

An alternative specification of the boundary conditions, which holds for all values of M , starts from the Stokes sectors for (1.1), which we denote by

$$\mathcal{S}_k = \left\{ x \in \mathbb{C} : \left| \arg(ix) - \frac{2\pi k}{2M+2} \right| < \frac{\pi}{2M+2} \right\}, \quad k \in \mathbb{Z}. \quad (1.3)$$

For all M the requirement (1.2) is equivalent to the demand that $\psi(x) \rightarrow 0$ as $x \rightarrow \infty$ in the sectors \mathcal{S}_{-1} and \mathcal{S}_1 . This allows for a convenient rephrasing of the eigenvalue condition in terms of the vanishing of a certain Wronskian. Following Hsieh and Sibuya [4–6], let $y_0(x, E, \alpha, \lambda)$ be the solution to (1.1) that is (uniquely) defined by the following asymptotic for $x \rightarrow \infty$ on the negative imaginary axis:

$$y_0(x, E, \alpha, \lambda) \sim \frac{i}{\sqrt{2}} (ix)^{-M/2-\alpha/2} \exp\left(-\frac{(ix)^{M+1}}{M+1}\right), \quad x \rightarrow -i\infty, \quad (1.4)$$

and then set

$$\omega = e^{i\pi/(M+1)} \quad (1.5)$$

and define a sequence of further solutions y_k to (1.1) by

$$y_k(x, E, \alpha, \lambda) = \omega^{k/2 - (-1)^k k\alpha/2} y_0(\omega^{-k} x, \omega^{-2Mk} E, (-1)^k \alpha, \lambda). \quad (1.6)$$

It is easily checked that y_k decays, or is subdominant, in \mathcal{S}_k , and that the ‘nearest-neighbour’ Wronskians $W[y_k, y_{k+1}] = y_k y'_{k+1} - y'_k y_{k+1}$ are all equal to 1.* The eigenvalue condition is then that y_{-1} and y_1 should be proportional to each other, in other words that E should be a zero of the ‘next-nearest-neighbour’ Wronskian

$$T(E, \alpha, \lambda) = W[y_{-1}, y_1]. \quad (1.7)$$

From this characterisation, and the analyticity of T as a function of its arguments, a number of important properties, such as the discreteness of the spectrum, immediately follow. In addition to being a spectral determinant, via the ODE/IM correspondence of [7] (see [8] for a review) T encodes the properties of the ground state of an integrable quantum field theory, in this case the Perk-Schultz model [9, 10]. This correspondence is based in part on the fact that T is a Stokes multiplier for (1.1), in that the following equation holds [1, 11]:

$$T(E, \alpha, \lambda) y_0(x, E, \alpha, \lambda) = y_{-1}(x, E, \alpha, \lambda) + y_1(x, E, \alpha, \lambda). \quad (1.8)$$

A feature the eigenvalue problem (1.2) shares with many other \mathcal{PT} -symmetric problems is the reality of its spectrum for many values of the free parameters. In particular, for real $M > 1$, α and λ , the spectrum of (1.1) can be proved to be

- *real* if $\alpha < M + 1 + 2|\lambda|$; (1.9)

- *positive* if $\alpha < M + 1 - 2|\lambda|$. (1.10)

These results were established in [1] using techniques inspired by the ODE/IM correspondence. One of the main aims of this paper is to refine this picture and to explore in more detail how and where spectral reality is lost as the region (1.9) is left.

Along the lines $\alpha = M + 1 \pm 2\lambda$ which form the frontiers of the region (1.9) of guaranteed reality, the model has an exactly-zero energy level, as in supersymmetric quantum mechanics. The ‘protection’ of this level can be seen as the mechanism by which the first levels become complex [2]. However, numerical investigations at $M = 3$, reported in [2], showed that the region within which the spectrum of (1.1) is complex has considerably more structure than (1.9) might suggest. The curved, cusped line of figure 2 indicates where the first pair of complex eigenvalues is formed as the region of complete spectral reality is left; it touches the lines $\alpha = M + 1 \pm 2\lambda$ at isolated points, where the protected zero-energy level coincides with another level.

*Note, a propagating typo in [1] and [8] resulted in the factor of $(-1)^k$ multiplying $k\alpha/2$ in the exponent of ω being omitted from the definition of y_k given in those papers. None of the other formulae in [1, 8] are affected.

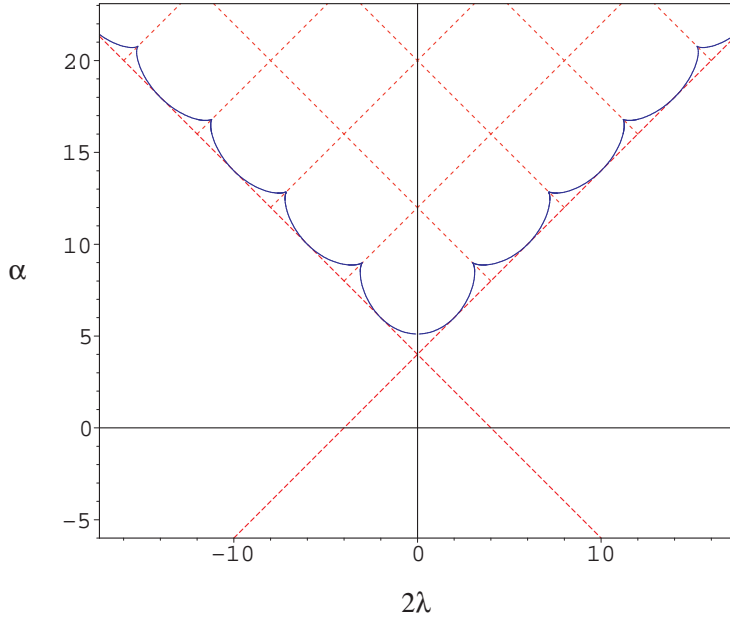


Figure 2: The domain of unreality in the $(2\lambda, \alpha)$ plane for $M = 3$, with portions of lines with a protected zero-energy level also shown. The horizontal axis is $2\lambda = 2l + 1$.

The additional dotted lines on the figure, also at angles of $\pm 45^\circ$, show points *within* the region $\alpha > M + 1 + 2|\lambda|$ where the model has an exactly-zero energy level; exceptionally for $M = 3$, the model is also quasi-exactly solvable along these lines. It is notable that, to within numerical accuracy, the cusps on the boundary of the region of unreality appear to lie exactly on these lines.

It is natural to ask where further pairs of complex eigenvalues are formed. For $M = 3$ the answer is shown in figure 3, adapted from [8]; the same pattern was found independently by Sorrell [12] via a complex WKB treatment of the problem. The pattern of cusps is repeated, with the cusps again appearing to lie on the lines of protected zero-energy levels.

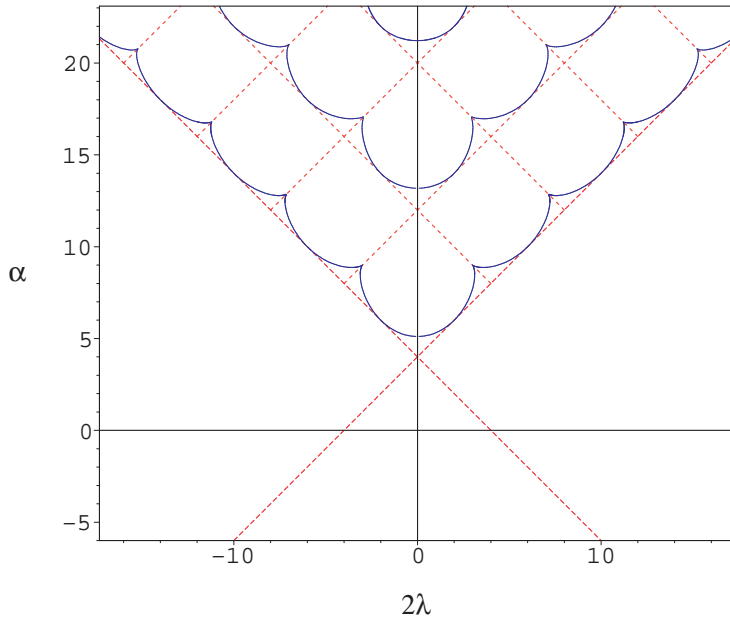


Figure 3: The $(2\lambda, \alpha)$ plane for $M = 3$, showing lines across which further pairs of complex eigenvalues are formed.

The analysis of [2] left a number of questions open. Whilst the merging and subsequent complexification of levels was suggestive of exceptional points and a Jordan block structure for the Hamiltonian, this was not demonstrated explicitly. The apparent siting of the cusps on lines with simultaneous quasi-exact solvability and protected zero-energy levels was not proved; in particular, it was not clear whether this feature should be associated with the zero-energy level (in which case it should persist for $M \neq 3$) or with the quasi-exact solvability (in which case it might be lost for $M \neq 3$). Finally, and connected with this last question, the general pattern away from $M = 3$ was not explored.

In this paper we revisit these issues. For $M = 3$ we investigate the positions of the cusps, proving that they do indeed lie on QES lines, and look at the exceptional points in the spectrum and the Jordan form at such points. We then explore the situation for $M \neq 3$ numerically, and verify the picture that emerges with detailed perturbative studies near $M = 1$ and $M = \infty$. The perturbative treatment near $M = 1$ also gives a new insight into the transition to infinitely-many complex eigenvalues for $M < 1$, first observed by Bender and Boettcher for the $\alpha = 0$, $\lambda^2 = \frac{1}{4}$ case of (1.1).

2 Exact locations of special exceptional points

2.1 Generalities and previous results

Exact formulae for the full curves of exceptional points are unlikely to exist, even for $M = 3$. However, certain exceptional points *can* be located exactly, and this information turns out to be very useful in mapping the full phase diagram. As in [2], we begin by introducing an alternative set of coordinates on the $(2\lambda, \alpha)$ plane, defined by

$$\alpha_{\pm} = \frac{1}{2M+2} [\alpha - M - 1 \pm 2\lambda]. \quad (2.1)$$

For $M = 3$ these coordinates are illustrated in figure 4. The lines $\alpha_+ \in \mathbb{N}$ and $\alpha_- \in \mathbb{N}$ correspond to the dotted lines on figures 2 and 3, along which the model (1.1) has an exactly-zero energy level. For $M = 3$ the existence of this level can be understood in terms of quasi-exact solvability and a hidden \mathcal{N} -fold supersymmetry [1, 13]. There are also exactly-zero energy levels along the lines $\alpha_{\pm} = 0$, related for all values of M to standard quantum-mechanical supersymmetry [2].

Exceptional points occur in the spectrum of an eigenvalue problem whenever the coalescence of two or more eigenvalues is accompanied by a coalescence of the corresponding eigenvectors; at such points there is a branching of the spectral surface [14–17]. In \mathcal{PT} -symmetric systems, eigenvalues are all either real, or in complex-conjugate pairs. Complex eigenvalues can therefore be formed only via the intermediate coincidence of two (or more) previously-real eigenvalues. For one-dimensional problems of the sort under discussion here genuine degeneracies of levels are impossible – since, for example, the Wronskian of any two solutions which both decay exponentially in the same asymptotic direction must vanish – and so levels in our problem can only coincide at exceptional points. Hence the cusped lines on figures 2 and 3 are lines of exceptional points. In fact, we shall see that points on the (codimension one) smooth segments of the cusped lines are quadratically exceptional, with two levels coalescing, while the cusps themselves, of codimension two, are cubic exceptional points. In the following, we will often refer to a connected union of quadratically-exceptional lines and cubically-exceptional points as an exceptional line.

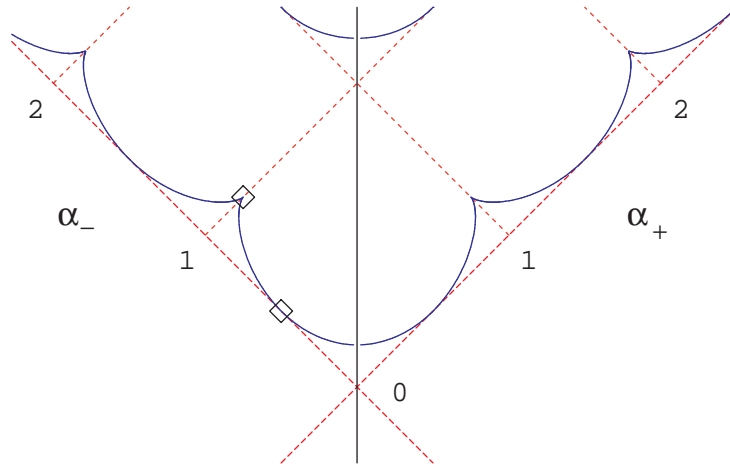


Figure 4: An enlarged view of the $M = 3$ phase diagram, showing the (α_+, α_-) coordinates. The boxes indicate the locations of the quadratic and cubic exceptional points, at $(\alpha_+, \alpha_-) = (0, 1/2)$ and $(1/4, 1)$, which are discussed later in the main text.

The exactly-zero energy levels can be used to control the pairing-off of eigenvalues and the associated formation of exceptional points [2]. On the ‘supersymmetric’ lines $\alpha_{\pm} = 0$ there is always at least one zero-energy eigenvalue, for any value of M . The points where this eigenvalue becomes degenerate with a second one can be found by looking for zero eigenvalues of the supersymmetric partner potential, the partner for $(\alpha_+, 0)$ being $(\alpha_+ - \frac{M-1}{M+1}, -1)$ and that for $(0, \alpha_-)$ being $(-1, \alpha_- - \frac{M-1}{M+1})$. This idea was used in [2] to show the existence of quadratic exceptional points for

$$(\alpha_+, \alpha_-) = (0, m - \frac{2}{M+1}) \quad \text{and} \quad (\alpha_+, \alpha_-) = (m - \frac{2}{M+1}, 0) \quad (2.2)$$

where $m \in \mathbb{N} \equiv \{1, 2, \dots\}$. At $M = 3$ these are the points on figure 2 where the cusped curve touches the lines $\alpha_{\pm} = 0$. For $M = 3$, a similar argument can be applied on the other lines $\alpha_{\pm} = n \in \mathbb{N}$ on which there is an exact zero-energy level, using a higher-order supersymmetry to eliminate this level together with $2n$ others [1, 2]. This establishes the existence of quadratic exceptional points at

$$(\alpha_+, \alpha_-) = (n, m - \frac{1}{2}) \quad \text{and} \quad (\alpha_+, \alpha_-) = (m - \frac{1}{2}, n), \quad m \in \mathbb{N}, \quad n \in \mathbb{Z}^+ \quad (M = 3). \quad (2.3)$$

These are the points on figure 3 where cusped curves touch the other lines $\alpha_{\pm} \in \mathbb{Z}^+$. In the next section we will generalise these results to other values of M .

2.2 Locating exceptional points using self-orthogonality

Our alternative argument starts from the idea, discussed in, for example, [16], that at an exceptional point at least one state will be self-orthogonal, in the sense that its inner product with itself under a suitable symmetric inner product must vanish. For the present paper we take this inner product to be

$$(f|g) \equiv \int_{\mathcal{C}} f(x)g(x) dx \quad (2.4)$$

where the contour \mathcal{C} is as in section 1. This inner product is bilinear rather than sesquilinear, and – at least in cases where the contour \mathcal{C} is the real axis – it is sometimes referred to as the c -product [18]. Correspondingly we will refer to $\sqrt{(f|f)}$ as the c -norm of f ; note that there is no need for this to be a real number. The c -product is well-defined for any pair of functions which decay exponentially as $|x| \rightarrow \infty$ along \mathcal{C} , and \mathcal{H} is symmetric with respect to it: $(f|\mathcal{H}g) = (\mathcal{H}f|g)$.

At an exceptional point, associated with some eigenvalue E , the Hamiltonian acquires a Jordan block form, and a so-called Jordan chain $\{\psi^{(0)} \dots \psi^{(k-1)}\}$ can be defined which spans the subspace of the k merging levels, such that

$$(\mathcal{H} - E)\psi^{(j)} = \psi^{(j-1)}, \quad j = 0 \dots k-1, \quad \psi^{(-1)} \equiv 0. \quad (2.5)$$

Then $(\psi^{(0)}|\psi^{(0)}) = (\psi^{(0)}|(\mathcal{H}-E)\psi^{(1)}) = ((\mathcal{H}-E)\psi^{(0)}|\psi^{(1)}) = 0$, and so the state $\psi^{(0)}$ is indeed self-orthogonal with respect to the c -product. Conversely, suppose that some eigenstate ψ , with eigenvalue E , has vanishing c -norm, so that $(\psi|\psi) = 0$. We would like to show that this implies that our system is lying at an exceptional point, and to this end we recall a useful result, previously exploited in this context by Trinh [19]. Suppose that E_n is an eigenvalue, so that y_{-1} and y_1 are proportional to each other and $T(E_n, \alpha, \lambda) = 0$. In fact, from (1.8), for such an E we have $y_{-1}(x, E, \alpha, \lambda) = -y_1(x, E, \alpha, \lambda)$. Writing $\psi = y_{-1} = -y_1$, the relevant result, converted to the normalisations used in this paper, is

$$(\psi|\psi)|_{E_n} = T'(E_n) \quad (2.6)$$

where the prime denotes differentiation with respect to E , and the dependence of T on α and λ has been left implicit. Now suppose that, as a function of some combination of α and λ , $(\psi|\psi)$ has an isolated zero. Then at this point, $T(E)$ as a function of E has a multiple zero which it does not possess in the neighbourhood of this point. The zero of $(\psi|\psi)$ must therefore mark a point where two or more eigenvalues of the eigenproblem have collided. Given the impossibility of genuine degeneracies in this problem, this must be an exceptional point, as claimed.

These results are useful in the present context because along the lines $\alpha_+ = n$ and $\alpha_- = n$, $n \in \mathbb{Z}^+$, one eigenfunction *can* be found exactly, namely that with eigenvalue $E = 0$. Consider the line $\alpha_- = n$, along which

$$\alpha - 2\lambda = (2n+1)(M+1). \quad (2.7)$$

(Corresponding results for the line $\alpha_+ = n$ can be obtained by negating λ throughout in the following.) Then the zero-energy eigenfunction $\psi = y_{-1} = -y_1$, normalised in line with (1.4) and (1.6), is

$$\psi(x) = \frac{1}{\sqrt{2}} \frac{n!(M+1)^n}{2^n} (ix)^{\frac{1}{2}+\lambda} L_n^{\left(\frac{2\lambda}{M+1}\right)} \left(\frac{-2(ix)^{M+1}}{M+1} \right) e^{(ix)^{M+1}/(M+1)} \quad (2.8)$$

where $L_n^{(\gamma)}(t)$ is the n^{th} generalised Laguerre polynomial. (To check that ψ has been normalised with the correct asymptotic, note the relation (2.7) between λ and α and the fact that the highest term of $L_n^{(\gamma)}(t)$ is $\frac{(-1)^n}{n!} t^n$.)

To evaluate $(\psi|\psi)$, we distort the contour \mathcal{C} to the union of rays $-\gamma_{-1} + \gamma_1$, where

$$\gamma_{\pm 1} = \left\{ x = \frac{1}{i} e^{\pm i\pi/(M+1)} t, t \in [0, \infty) \right\}, \quad (2.9)$$

and then use the integral (C.1), analytically continuing in λ if necessary to ensure convergence. The final result is

$$(\psi|\psi) = \frac{\pi}{2} \left(\frac{M+1}{2} \right)^{2n-1+\frac{2\lambda+2}{M+1}} \frac{1}{\Gamma\left(1 - \frac{2+2\lambda}{M+1}\right)} Q_n(\lambda) \quad (2.10)$$

where $Q_n(\lambda)$ is a polynomial of degree n in λ , which can be expressed in terms of the hypergeometric function ${}_3F_2$ and Pochhammer symbols $(x)_k \equiv x(x+1) \dots (x+k-1)_k$ as

$$\begin{aligned} Q_n(\lambda) &= \left(1 - \frac{2}{M+1}\right)_n \left(1 + \frac{2\lambda}{M+1}\right)_n {}_3F_2\left(-n, \frac{2\lambda+2}{M+1}, \frac{2}{M+1}; 1 + \frac{2\lambda}{M+1}, -n + \frac{2}{M+1}; 1\right) \\ &= \sum_{k=0}^n (-1)^k \binom{n}{k} \left(1 - \frac{2}{M+1} - k\right)_n \left(\frac{2\lambda+2}{M+1}\right)_k \left(1 + \frac{2\lambda}{M+1} + k\right)_{n-k}. \end{aligned} \quad (2.11)$$

The zeros of (2.10) locate all those exceptional points on the line $\alpha_- = n$ which involve the merging of levels at the eigenvalue $E = 0$. For $M = 3$, we will argue in the next subsection that this captures *all* exceptional points on this line, with the zeros of $Q_n(\lambda)$ being the cubic exceptional points associated with cusps on the phase diagram. For other values of M , as will be described in more detail in section 4, the cubic exceptional points move away from the lines $\alpha_{\pm} = n$, to be replaced on these lines by pairs of quadratic exceptional points, only one of each pair being at $E = 0$ and corresponding to a zero of $Q_n(\lambda)$.

By contrast, the infinitely-many zeros of the factor $1/\Gamma(1 - \frac{2+2\lambda}{M+1})$ in (2.10) *always* correspond to quadratic exceptional points. These zeros are at

$$2\lambda = (M+1)m - 2, \quad m \in \mathbb{N} \quad (2.12)$$

and using (2.7) they imply the existence of exceptional points at

$$(\alpha_+, \alpha_-) = (n + m - \frac{2}{M+1}, n), \quad m \in \mathbb{N}, \quad n \in \mathbb{Z}^+. \quad (2.13)$$

This result matches and extends the previously-known cases: for $n = 0$, it yields the points (2.2), found in [2] using ideas based on supersymmetry, while for $M = 3$ the result (2.3) is reproduced.

2.3 Locating exceptional points using quasi-exact solvability

Self-orthogonality yields important information about the phase diagram at general M , but it fails to identify the degrees of exceptional points, and it only sees exceptional points which have eigenvalue zero. In this subsection we describe a complementary tactic, special to $M = 3$, which avoids these problems by exploiting the fact that for $M = 3$ the model is quasi-exactly solvable (QES) on the lines $\alpha_{\pm} \in \mathbb{N}$. This will allow us to prove some general statements about the spectrum of the model on these lines. A key part of the argument, established in [2], is that any complex levels on the lines $\alpha_{\pm} \in \mathbb{N}$ must lie in the QES sector of the model.

For the rest of this section and all of the next we therefore restrict to $M = 3$, and, to minimise the proliferation of factors of i , we replace x by $z = ix$ and set $\Phi(z) = \psi(z/i)$. The quantisation contour is also rotated by 90° , and the eigenproblem (1.1) becomes

$$\left[-\frac{d^2}{dz^2} + z^6 + \alpha z^2 + \frac{\lambda^2 - \frac{1}{4}}{z^2} \right] \Phi(z) = -E \Phi(z), \quad \Phi(z) \in L^2(i\mathcal{C}). \quad (2.14)$$

A choice for the contour $i\mathcal{C}$ which avoids all singularities in the wavefunctions is given in equation (3.3) below; alternatively a rotated version of (2.9) can be used, with suitable analytic continuations whenever divergent integrals are encountered.

If boundary conditions had been imposed at $z = 0$ and $z = +\infty$, the problem (2.14) would have been quasi-exactly solvable whenever α and λ were related by $\alpha = -(4J + 2\lambda)$ for some positive integer J , with J energy levels exactly computable [20]. Bender and Dunne [21] found an elegant method to find the corresponding wavefunctions, square integrable along the positive real axis. We are instead interested in solutions defined along the contour $i\mathcal{C}$, but with minor modifications the approach of [21] can still be used[†]. We set $J = \alpha/4 - \lambda/2$ and look for solutions of the form

$$\Phi(z) = e^{\frac{z^4}{4}} z^{\lambda + \frac{1}{2}} \sum_{n=0}^{\infty} a_n(\lambda) p_n(E, \lambda, J) z^{2n} \quad (2.15)$$

where

$$a_n(\lambda) = \left(-\frac{1}{4} \right)^n \frac{1}{n! \Gamma(n + \lambda + 1)}. \quad (2.16)$$

The function $\Phi(z)$ will solve (2.14) if the coefficients $p_n(E, \lambda, J)$ satisfy the recursion relation

$$p_n = -E p_{n-1} + 16(J - n + 1)(n - 1)(n - 1 + \lambda) p_{n-2}, \quad n \geq 1. \quad (2.17)$$

[†]For earlier discussions of quasi-exactly solvable \mathcal{PT} -symmetric sextic potentials, see [1, 2, 22].

Setting $p_0 = 1$ fixes the normalisation, and then $p_1 = -E$ follows from (2.17) at $n = 1$. If J is a positive integer, then the second term on the RHS of (2.17) vanishes when $n = J + 1$, and so p_{J+1} is proportional to p_J , as are all subsequent coefficients $p_{m>J+1}$. At a zero of p_J the series therefore terminates. Owing to the sign of the argument of the exponential prefactor in (2.15) (opposite to that in [21]), the corresponding $\Phi(z)$ will automatically satisfy the revised boundary conditions. We define the J^{th} Bender-Dunne polynomial for this problem to be

$$P_J(E, \lambda) = p_J(E, \lambda, J) . \quad (2.18)$$

This is a polynomial of degree J in E , and degree $J - 1$ in λ . By the above reasoning, its zeros in E give the J quasi-exactly solvable (QES) levels that the model possesses on the line $\alpha = 4J + 2\lambda$. Since boundary conditions are not imposed at the origin, replacing λ by $-\lambda$ throughout also leads to an acceptable solution, and so for each $J \in \mathbb{N}$ there are two lines of quasi-exact solvability in the $(2\lambda, \alpha)$ plane: $\alpha = 4J + 2\lambda$ and $\alpha = 4J - 2\lambda$. In the (α_+, α_-) coordinates these lines are $(\alpha_+, \alpha_-) = (\frac{1}{2}(J-1+\lambda), \frac{1}{2}(J-1))$ and $(\frac{1}{2}(J-1), \frac{1}{2}(J-1-\lambda))$ respectively. Figure 6, below, shows the QES lines on the $(2\lambda, \alpha)$ plane.

These lines are very useful in mapping the exceptional points on the whole $(2\lambda, \alpha)$ plane. The reasoning is best explained via a sequence of lemmas, which may be of independent interest.

Lemma 1: The Bender-Dunne polynomials satisfy the ‘reflection symmetry’

$$P_J(E, \lambda) = (-i)^J P_J(iE, -J - \lambda) \quad (2.19)$$

Proof: Introduce a set of polynomials defined by $r_n(E, \lambda, J) = (-i)^n p_n(iE, -J - \lambda, J)$. Direct substitution into (2.17) shows that the r_n satisfy the recursion

$$r_n = -E r_{n-1} + 16(J - n + 1)(n - 1)(J - n + 1 + \lambda)r_{n-2}, \quad n \geq 1 \quad (2.20)$$

with initial conditions $r_{-1} = 0$, $r_0 = 1$. The claimed symmetry is equivalent to $r_J(E, \lambda, J) = p_J(E, \lambda, J)$. Now consider a more general recursion

$$u_n = -E u_{n-1} + b_{n-1} u_{n-2}, \quad n \geq 1, u_{-1} = 0, u_0 = 1 \quad (2.21)$$

with some set of coefficients $\{b_n\}$. It is straightforward to verify that the general solution is

$$u_n = (-1)^n \sum_{k=0}^{\lfloor n/2 \rfloor} \left(\sum_{\substack{\{0 < i_1 < \dots < i_k < n\} \\ |i_{j+1} - i_j| > 1}} b_{i_1} b_{i_2} \dots b_{i_k} \right) E^{n-2k} . \quad (2.22)$$

In particular, p_J is given by (2.22) with $n = J$ and $b_i = 16(J - i + 1)(i - 1)(i - 1 + \lambda)$, and r_J by (2.22) with $n = J$ and $b_i = 16(J - i + 1)(i - 1)(J - i + 1 - \lambda)$. Thus the two differ by the substitution $b_i \rightarrow b_{J-i}$, and since (2.22) for $n = J$ is itself symmetrical under this mapping, the lemma is proved.

Lemma 2: If $\lambda < 1 - J$, then all zeros of $P_J(E, \lambda)$ are real and distinct.

Proof: The given values of λ correspond to the points on the QES line $\alpha = 4J + 2\lambda$ which lie in the region $\alpha < 4 + 2|\lambda|$. The reality result (1.9) then implies that the spectrum of the eigenproblem (2.14), which includes the QES sector described by the zeros of $P_J(E, \lambda)$, is real. These zeros must therefore all be real. To show that the zeros are simple, we use the fifth spectral equivalence from [1] to map our problem on to one which, for the given range of λ , is hermitian. Converted into the current coordinates, this equivalence states that the spectrum of (2.14) is the same as that of the following radial problem for functions defined on \mathbb{R}^+ and decaying at $x \rightarrow +\infty$:

$$\left[-\frac{d^2}{dx^2} + x^6 + \alpha' x^2 + \frac{\lambda'^2 - \frac{1}{4}}{x^2} \right] \phi(x) = E \phi(x), \quad \phi(x)|_{x \rightarrow 0} \sim x^{\lambda'+1/2}, \quad (2.23)$$

Lemma 4: On the infinite segment $\lambda > -1$ of the QES line $\alpha = 4J + 2\lambda$, the eigenproblem (2.14) has exactly J distinct non-real (in fact purely imaginary) eigenvalues for J even, and $J-1$ non-real (and purely imaginary) eigenvalues and 1 zero eigenvalue for J odd. By the $\lambda \rightarrow -\lambda$ symmetry of the problem, the same holds for the $\lambda < -1$ segment of the $\alpha = 4J - 2\lambda$ QES line.

Proof: First recall from [2] that on QES lines, the non-QES sector of the spectrum is entirely real. The result then follows on combining lemma 3 with the fact that the degree J polynomial $P_J(E, \lambda)$ is a function of E^2 for J even, and E times a function of E^2 for J odd.

The results so far show that on the QES lines $\alpha = 4J + 2\lambda$ the spectrum is entirely real for $\lambda < -J + 1$, and has exactly $2[J/2]$ complex eigenvalues for $\lambda > -1$, where $[x]$ denotes the largest integer less than or equal to x . This is illustrated in figure 6.

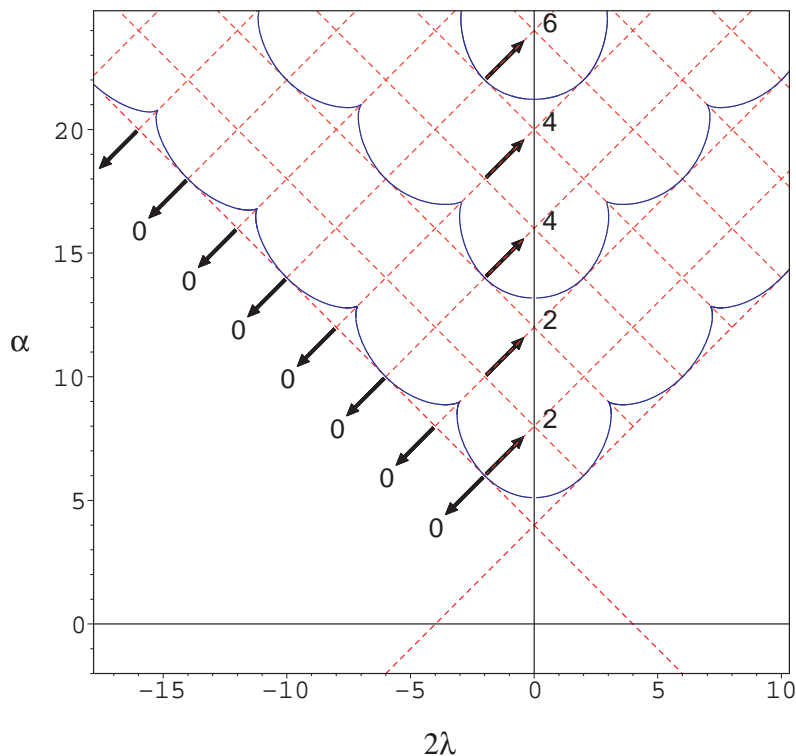


Figure 6: The lines $\alpha = 4J \pm 2\lambda$, $J \in \mathbb{N}$, of quasi-exact solvability on the $(2\lambda, \alpha)$ plane. The arrows indicate the (open) segments of the lines $\alpha = 4J + 2\lambda$ on which the precise numbers of non-real eigenvalues are determined by lemmas 2 and 4. Note that these results are consistent with the locations of the numerically-obtained curved cusped lines (blue online), across each of which the number of non-real eigenvalues increases by two. For $J \neq 1$, only those parts of the QES lines which lie in the zone of possible unreality $\alpha > 4 + 2|\lambda|$ are shown. The lines with J odd coincide with the protected zero-energy level lines shown in figures 2, 3 and 4.

The situation in the remaining intervals $-J + 1 \leq \lambda \leq -1$ is clarified by lemmas 5 and 6.

Lemma 5: At the points $\lambda = -J + n$, $n = 2 \dots J-1$ on the QES line $\alpha = 4J + 2\lambda$, the problem has exactly $2[n/2]$ distinct non-real eigenvalues.

Proof: In addition to being on the line $\alpha = 4J + 2\lambda$, the given points lie on the lines $\alpha = 4n - 2\lambda$ in a region where lemma 4 applies.

Lemma 6: On each segment $-J + 2m - 1 \leq \lambda \leq -J + 2m$ of the QES line $\alpha = 4J + 2\lambda$, where $J \geq 2$ and $m = 1, 2 \dots [(J+1)/2] - 1$, there is at least one point where the eigenproblem has an exceptional point with eigenvalue zero. The same is true of the segments $J - 2m \leq \lambda \leq J - 2m + 1$, $m = 1, 2 \dots [(J+1)/2] - 1$ of the QES line $\alpha = 4J - 2\lambda$.

Proof: By lemma 5, when $\lambda = -J + 2m - 1$ the number of non-real eigenvalues is $2m - 2$, while

when $\lambda = -J + 2m$ it is $2m$. The number of non-real eigenvalues thus changes by two as λ moves from $-J + 2m - 1$ to $-J + 2m$. By the \mathcal{PT} symmetry of the problem, non-real eigenvalues always occur in complex-conjugate pairs; combining this with the $E \rightarrow -E$ symmetry of the QES sector, any non-real eigenvalues created or destroyed away from $E = 0$ must appear in quartets. So to change the number of non-real eigenvalues by two, at least one pair must be created or destroyed at zero, and hence there must be at least one exceptional point with eigenvalue zero in each interval $-J + 2m - 1 \leq \lambda \leq -J + 2m$. The final statement of the lemma then follows from the $\lambda \rightarrow -\lambda$ symmetry of the problem.

Lemma 7: For $M = 3$, the zeros of the polynomials $Q_n(\lambda)$, defined in equation (2.11) above, are all real and simple, with one in each interval $\lambda \in [2m-1, 2m]$, $m = 1 \dots n$.

Proof: Specialising the discussion of subsection 2.2 to $M = 3$, $Q_n(\lambda)$ has a real zero at every point on the line $\alpha = 4(2n+1) + 2\lambda$, $\lambda \in \mathbb{R}$ where the eigenproblem has an exceptional point with eigenvalue zero. Combining this with lemma 6 taken at $J = 2n + 1$, $Q_n(\lambda)$ has at least one real zero in each interval $[2m-1, 2m]$, $m = 1 \dots n$; but since $Q_n(\lambda)$ is a polynomial of degree n this must exhaust all of its zeros, which must therefore also all occur singly.

Lemmas 6 and 7 show that on the lines $\alpha = 4J \pm 2\lambda$ with $J = 2n + 1$, there are n odd-order exceptional points with eigenvalue zero. If all of these have the lowest possible degree, that is three, then at each a pair of complex eigenvalues is created, and would account precisely for the total number of complex QES levels which must appear as the QES line is traversed. In principle, one could imagine more complicated scenarios where further pairs of complex levels appear at these exceptional points and then annihilate with each other later, but our numerical results show no evidence of such behaviour and we shall proceed on the assumption that it does not occur. If we further assume that the triply-exceptional points are isolated in the sense that there are no other triply-exceptional points in their immediate neighbourhoods in the $(2\lambda, \alpha)$ plane, then these points must be occurring where two lines of double degeneracy meet at a cusp, as illustrated in figure 7 below. Thus, subject to the two assumptions just mentioned, we have proved that for $M = 3$ the cusps in the exceptional lines do indeed lie on the lines of protected zero-energy levels, as conjectured earlier.

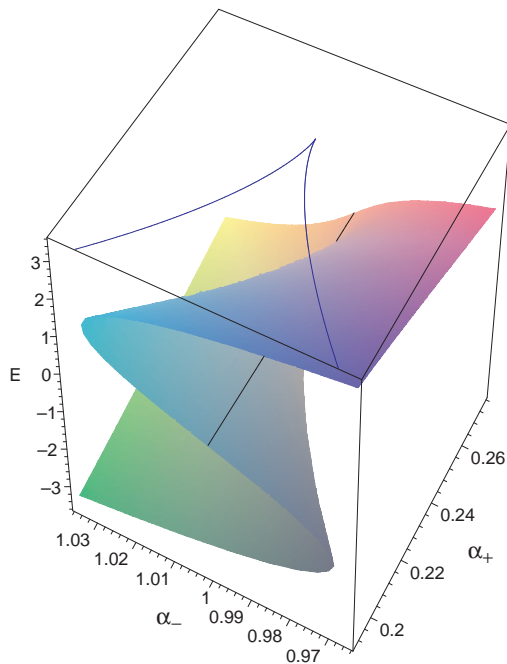


Figure 7: The behaviour of the energy level surface $E(\alpha_+, \alpha_-)$ in the vicinity of a cubic exceptional point.

The above results capture the $[J/2]$ transitions to complex levels that occur as the QES line $\alpha = 4J + 2\lambda$ is traversed, at each of which a pair of complex levels is created. However this does not necessarily exhaust all of the exceptional points on the corresponding QES line – indeed, for J odd (2.12) shows that there are infinitely-many more exceptional points on the line $\alpha = 4J + 2\lambda$, at $(2\lambda, \alpha) = (4m-2, 4J+4m-2)$, $m \in \mathbb{N}$. Examination of figure 6 reveals that at each of these points an exceptional line touches, but does not cross, the QES line, so that the exceptional point does not cause the creation of further complex levels while motion is restricted to the QES line. Once the QES line is left, the J QES levels start to mix with the non-QES sector, and further complex levels can be formed. (In fact, if the point $(4m-2, 4J+4m-2)$ on the QES line $\alpha = 4J + 2\lambda$ is left in a direction perpendicular to that line, a pair of complex levels is created in a *different* QES sector, that for the QES line $\alpha = 4(J+2m-1) - 2\lambda$.) This general picture, and also the claimed isolation of the triply-exceptional points as illustrated in figure 7, will be supported by some perturbative calculations in the next section.

One would also like to be able to rule out the more exotic scenarios for the behaviour of levels in the QES sector, mentioned in the discussion following lemma 7. We do not have a rigorous argument for this, but we do have extensive numerical, and some analytical, evidence for the following conjecture which, if true, would eliminate such possibilities:

Conjecture: For all λ , the squared zeros (in E) of the Bender-Dunne polynomials $P_J(E, \lambda)$ are real, and, apart from the zero at $E = 0$ when J is odd, they are monotonically-decreasing functions of λ .

Immediate consequences of a proof of the conjecture would be that QES levels, once complex, remain so, and that the only way that QES levels can become complex is via $E = 0$. In turn this would prove that the zeros of the polynomials $Q_n(\lambda)$ do indeed correspond to triply-degenerate points in the spectrum, since one can easily rule out the presence of zero eigenvalues in the non-QES sector at the relevant points.

The conjecture is similar in spirit to the Feynman-Hellman theorem, but the eigenproblem here is not hermitian, and this invalidates any variant of the standard proof. Note also that the conjecture is certainly false for the non-QES part of the spectrum, the (un-squared) levels of which can pass through zero while remaining real. As a sample of our numerical checks, figures 8 and 9 show the squared QES levels for $J = 20$ and $J = 21$. Apart from the $E^2 = 0$ line on figure 9, all the curves are monotonic; given this, the fact that they all pass through zero between $\lambda = 1 - J$ and $\lambda = -1$ follows from lemmas 2 and 3 above.

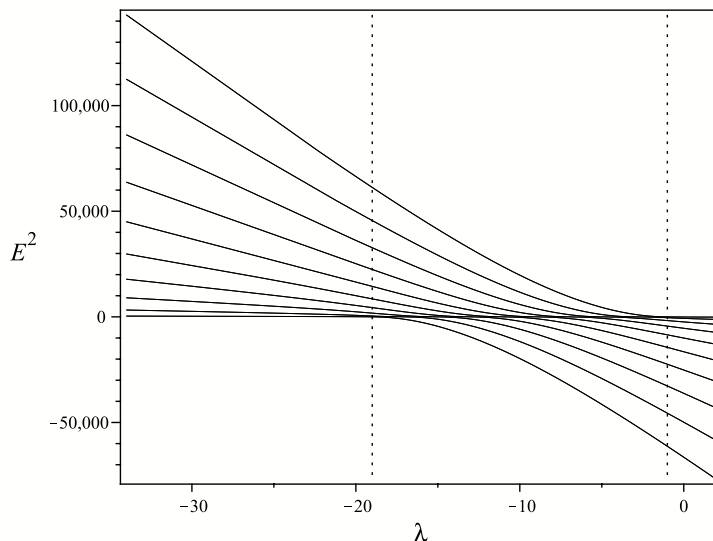


Figure 8: Squared QES levels for $J = 20$. The dotted vertical lines are at $\lambda = 1 - J$ and $\lambda = -1$; all transitions from real to imaginary eigenvalues occur for $1 - J \leq \lambda \leq -1$.

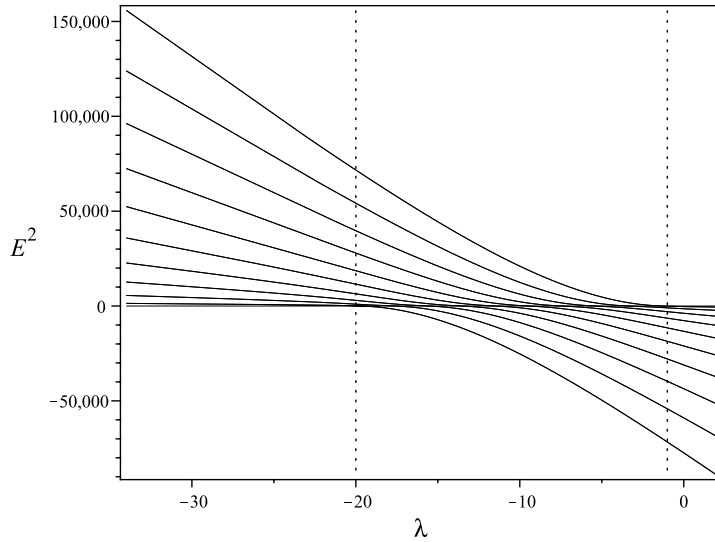


Figure 9: As figure 8, but for $J = 21$. Again, all transitions to imaginary eigenvalues occur for $1 - J \leq \lambda \leq -1$.

The curves shown on figures 8 and 9 appear to asymptote to linear functions of λ as $\lambda \rightarrow \pm\infty$. This turns out to be the case, as will be shown below, where the slopes of these functions will also be found exactly. Figures 10 and 11 illustrate these results, and further support the monotonicity conjecture, by plotting the derivatives of the squared QES levels, again for $J = 20$ and $J = 21$.

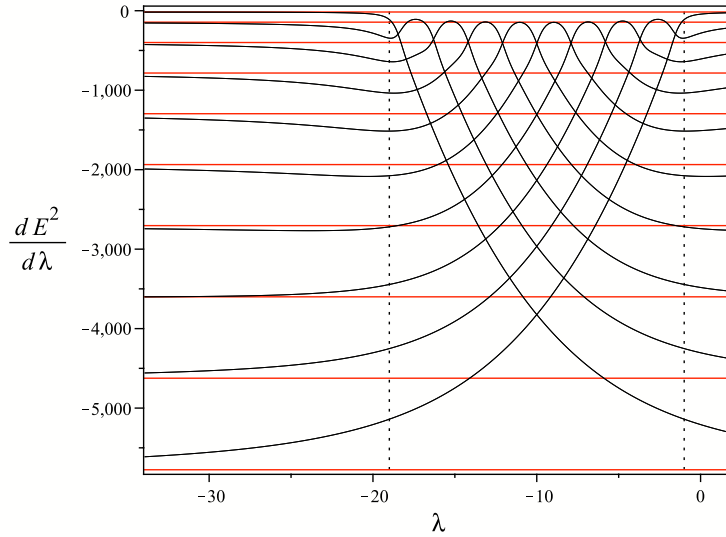


Figure 10: Derivatives of squared QES levels for $J = 20$. The straight horizontal lines (red online) show the predicted asymptotic values for these derivatives, which are everywhere negative. The symmetry of the plot about $\lambda = J/2$ follows from the reflection symmetry proved in lemma 1.

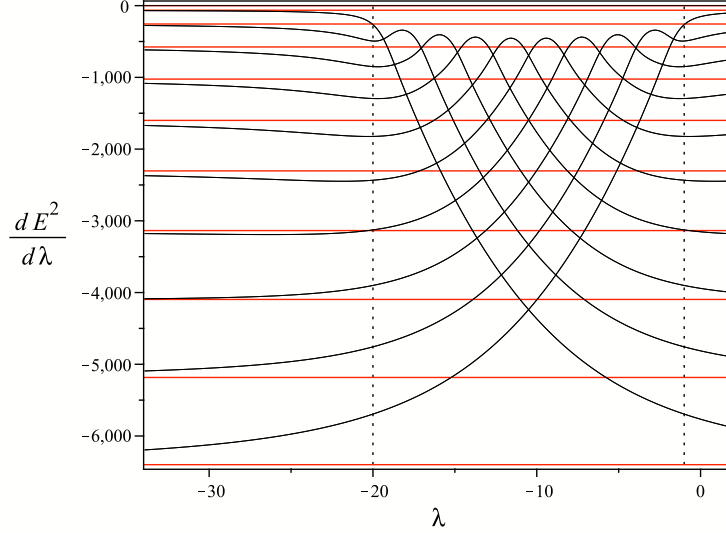


Figure 11: As figure 10, but for $J = 21$. All but one of the plotted functions are negative, the exception corresponding to the level at $E = 0$.

To treat the large- $|\lambda|$ behaviour of the QES levels analytically, a first approach is to return to the Bender-Dunne recursion relation (2.17). In the limit $|\lambda| \gg J$, and keeping $n \leq J$, this simplifies to

$$p_n = -E p_{n-1} + 16\lambda(J-n+1)(n-1)p_{n-2}, \quad p_0 = 1. \quad (2.27)$$

Solving for low-lying values of J , a remarkable simplification occurs precisely at $n = J$, where the asymptotic Bender-Dunne polynomials P_J^{asympt} are found. For J even,

$$P_J^{\text{asympt}}(E) = \prod_{k=1}^{J/2} (E^2 + 16(2k-1)^2\lambda), \quad (2.28)$$

while for J odd,

$$P_J^{\text{asympt}}(E) = -E \prod_{k=1}^{(J-1)/2} (E^2 + 16(2k)^2\lambda). \quad (2.29)$$

Hence the squared QES levels are indeed linear functions of λ in this limit, with slopes which are negative, and proportional to the squares of odd or even integers. Rather than prove these formulae directly from the asymptotic Bender-Dunne recursion relation, we will use the same spectral equivalence as employed in the proof of lemma 2 above. The polynomial $P_J(E, \lambda)$ encodes in its zeros the QES levels along the line $\alpha = 4J + 2\lambda$; by the reflection symmetry (2.19) it will suffice to consider the asymptotic behaviour of the levels in just one direction, which we choose to be $\lambda \rightarrow -\infty$. Then, instead of applying the mapping (2.24) immediately, we precede it by the trivial symmetry $(2\lambda, \alpha) \rightarrow (-2\lambda, \alpha)$ of the \mathcal{PT} -symmetric problems, which flips between the two QES lines shown on the left-hand diagram of figure 5. The line $(2\lambda, 4J + 2\lambda)$, $\lambda \in \mathbb{R}$, is now mapped to $(-2J, -4\lambda)$ on the $(2\lambda', \alpha')$ plane, the vertical line on the right-hand diagram of figure 5. The limit $\lambda \rightarrow -\infty$ is thus mapped to $\alpha' \rightarrow +\infty$, $2\lambda' = -2J$ in the spectrally-equivalent lateral problem (2.23). For the QES sector, we are only interested in the J lowest-lying levels, where J remains fixed as $\alpha' = -4\lambda \rightarrow +\infty$. In this limit the quadratic term in (2.23) comes to dominate and the problem reduces to the (scaled) radial simple harmonic oscillator

$$\left[-\frac{d^2}{dx^2} - 4\lambda x^2 + \frac{J^2 - \frac{1}{4}}{x^2} \right] \phi(x) = E \phi(x), \quad \phi(x)|_{x \rightarrow 0} \sim x^{-J+1/2}. \quad (2.30)$$

Since $J \geq 1$, the boundary conditions at the origin are irregular. Nevertheless, the problem can be solved exactly for any value of J , the first J levels being

$$E = \sqrt{-4\lambda}(-2J + 4n - 2), \quad n = 1, 2, \dots, J. \quad (2.31)$$

(Strictly speaking, a resonance when J is an integer means it is safest to shift J slightly away from integer values for the calculation, but the final result is unaffected.) It is straightforward to see that this confirms equations (2.28) and (2.29) above, as desired. (The overall normalisation of $P_J^{\text{asympt}}(E)$ can be fixed by considering the coefficient of E^J .) Note that these results imply the truth of the monotonicity conjecture in the limits $|\lambda| \rightarrow \infty$ and thus give some supporting evidence for its general validity. Unfortunately, the regions $|\lambda| \rightarrow \infty$ are not of interest from the point of view of reality properties, since they are already covered by lemmas 2 and 3 above, and so a full proof of monotonicity of the squared eigenvalues would still be worthwhile.

Finally, an alternative way to locate the cusps corresponding to the collision of levels at $E = 0$ is to examine the odd Bender-Dunne polynomials $P_{2m+1}(E, \lambda)$ directly. These factorise as E times a polynomial in E^2 , and there will be a multiply-degenerate zero-energy level whenever this polynomial vanishes at $E = 0$, or equivalently whenever

$$\left. \frac{d}{dE} P_{2m+1}(E, \lambda) \right|_{E=0} = 0. \quad (2.32)$$

For fixed m and $J \equiv 2m + 1$, consider the sequence of polynomials $p_{2n+1}(E, \lambda, J)$, $n = 0 \dots m$, and define

$$q_n(\lambda, m) = \frac{-1}{2^{7n} n!} \left. \frac{d}{dE} p_{2n+1}(E, \lambda, 2m+1) \right|_{E=0}. \quad (2.33)$$

A consideration of the Bender-Dunne recurrence (2.17) and its derivative at $E = 0$ shows that $q_n(\lambda, m)$ satisfies the first order recurrence

$$q_n = (m - n + \frac{1}{2})(n + \frac{1}{2}\lambda)q_{n-1} + \binom{m}{n} \prod_{k=1}^n (k - \frac{1}{2})(k - \frac{1}{2} + \frac{1}{2}\lambda), \quad (2.34)$$

with initial condition $q_0 = 1$. Anticipating the final result in our notation, we set

$$Q_m(\lambda) = q_m(\lambda, m) \quad (2.35)$$

so that $Q_m(\lambda)$ is a polynomial in λ of degree m , and its zeros are the points identified by (2.32). For example:

$$Q_1(\lambda) = \frac{1}{4}(3 + 2\lambda) \quad (2.36)$$

$$Q_2(\lambda) = \frac{1}{16}(41 + 40\lambda + 8\lambda^2) \quad (2.37)$$

$$Q_3(\lambda) = \frac{3}{64}(7 + 2\lambda)(63 + 56\lambda + 8\lambda^2). \quad (2.38)$$

It turns out that the general solution to (2.34) can be expressed using the hypergeometric function ${}_3F_2$ and Pochhammer symbols $(x)_k \equiv x(x+1)\dots(x+k-1)$, $(x)_k = (-1)^k(1-k-x)_k$. For $n = m$ this solution is

$$\begin{aligned} Q_m(\lambda) &= (1 + \frac{1}{2}\lambda)_m (\frac{1}{2})_m {}_3F_2(-m, \frac{1}{2}, \frac{1}{2} + \frac{1}{2}\lambda; 1 + \frac{1}{2}\lambda, \frac{1}{2} - m; 1) \\ &= \sum_{k=0}^m (-1)^k \binom{m}{k} (\frac{1}{2} - k)_m (\frac{1}{2} + \frac{1}{2}\lambda)_k (1 + \frac{1}{2}\lambda + k)_{m-k}. \end{aligned} \quad (2.39)$$

This is the $M = 3$ case of the general formula (2.11), here derived by a completely different route. Since terms being summed in (2.39) are invariant up to a factor of $(-1)^m$ under the simultaneous

α_+	α_-
1	$\frac{1}{4}$
2	$\frac{3}{4} \pm \frac{3\sqrt{2}}{8}$
3	$\frac{5}{4}, \frac{5}{4} \pm \frac{\sqrt{70}}{8}$
4	$\frac{7}{4} \pm \frac{\sqrt{86+5\sqrt{190}}}{8}, \frac{7}{4} \pm \frac{\sqrt{86-5\sqrt{190}}}{8}$
5	$\frac{9}{4}, \frac{9}{4} \pm \frac{\sqrt{170+7\sqrt{214}}}{8}, \frac{9}{4} \pm \frac{\sqrt{170-7\sqrt{214}}}{8}$

Table 1: Location of some of the cusps in the (α_+, α_-) -plane for $M = 3$.

exchange $k \rightarrow m-k$, $\lambda \rightarrow -2m-1-\lambda$, the $M = 3$ polynomial $Q_m(\lambda)$ is invariant up to a sign under $\lambda \rightarrow -2m-1-\lambda$ and its zeros are symmetrically distributed about $\lambda = -m - 1/2$. This reflects the more general result (2.19). For m odd, this means that $Q_m(-m - 1/2) = 0$.

Returning to the α_{\pm} coordinates, if $J = 2m+1$ and $m \in \mathbb{N}$ then the QES line $\alpha = 4J + 2\lambda$ corresponds to $(\alpha_+, \alpha_-) = (m+\lambda/2, m)$, and the m cusps on this line occur at the zeros of $Q_m(\lambda)$, while for $\alpha = 4J - 2\lambda$ the cusps lie on the line $(\alpha_+, \alpha_-) = (m, m-\lambda/2)$ with λ a zero of $Q_m(-\lambda)$. The first few cases from this second set are given in table 1; to within our numerical accuracy, they match the cusp positions shown in figure 3. Notice that the symmetrical distribution of the zeros of $Q_m(\lambda)$ mentioned at the end of the last paragraph implies a relationship between the locations of pairs of a priori unrelated cusps and gives a simple formula for the remaining ‘unpaired’ cusps: $(\alpha_+, \alpha_-) = (m, m/2-1/4)$ and $(\alpha_+, \alpha_-) = (m/2-1/4, m)$ for all odd $m \in \mathbb{N}$.

3 Jordan blocks for $M = 3$

3.1 The Jordan block at a quadratic exceptional point

We now investigate the exceptional points and their neighbourhoods in more detail, beginning with a quadratic example. The first step is to find the Hamiltonian H_0 at the exceptional point, restricted to the two-dimensional space of states which merge at that point. This will have a Jordan block form. We then perturb about this point by writing the full Hamiltonian, H , as $H = H_0 + V$, and expand H using the wavefunctions of H_0 as a basis. Thus we will need to calculate

$$H_{mn} = \langle \tilde{\phi}_m | H | \phi_n \rangle = \langle \tilde{\phi}_m | H_0 | \phi_n \rangle + \langle \tilde{\phi}_m | V | \phi_n \rangle, \quad (3.1)$$

where $\{\phi_m, \phi_n\}$ is a basis for the Jordan block form of H_0 , and $\{\tilde{\phi}_m, \tilde{\phi}_n\}$ is an appropriate dual basis, so that the functions together form a part of a biorthogonal system, as discussed in [23] for generic cases and [16] in the presence of exceptional points. In the current setting, wavefunctions decay as $|z| \rightarrow \infty$ along $i\mathcal{C}$ and a suitable pairing between functions $g(z)$ and ‘dual functions’ [23] $\tilde{f}(z)$ is a rotated version of the c -product (2.4):

$$\langle \tilde{f} | g \rangle = \int_{i\mathcal{C}} \tilde{f}(z) g(z) dz. \quad (3.2)$$

Here and below a convenient choice for $i\mathcal{C}$, beginning and ending in the (rotated) Stokes sectors $i\mathcal{S}_{-1}$ and $i\mathcal{S}_1$, will be

$$i\mathcal{C} = -\gamma_{-1} + \gamma_0 + \gamma_1 \quad (3.3)$$

where $\gamma_{\pm 1} = \{te^{\pm\pi i/4}, t \in [\varepsilon, \infty)\}$, $\gamma_0 = \{\varepsilon e^{it}, t \in [-\pi/4, \pi/4]\}$, and the small positive number ε ensures that any singularities at $z = 0$ are avoided. For later use we note the following basic integral along the contour $i\mathcal{C}$, which holds for arbitrary $a \in \mathbb{R}$:

$$\int_{i\mathcal{C}} z^a e^{z^4/2} dz = \frac{2^{(a-3)/4} \pi i}{\Gamma(\frac{1}{4}(3-a))}. \quad (3.4)$$

This is easily checked, either by analytic continuation from $a > -1$ or using the real integral $\int_{\epsilon}^{\infty} t^a e^{-t^4/2} dt = 2^{(a-7)/4} \Gamma(\frac{1}{4}(a+1), \frac{1}{2}\epsilon^4)$, where $\Gamma(a, z)$ is the incomplete gamma function.

As our example we take the exceptional point at $(2\lambda, \alpha) = (2, 6)$, $(\alpha_+, \alpha_-) = (1/2, 0)$, shown with a box on figure 4. This lies on two lines of quasi-exact solvability, $(\alpha = 4J + 2\lambda)|_{J=1}$ and $(\alpha = 4J - 2\lambda)|_{J=2}$, and we shall focus on the second of these. Along this line $\alpha = 8 - 2\lambda$ and the eigenvalue problem is

$$\left(-\frac{d^2}{dz^2} + z^6 + (8 - 2\lambda)z^2 + \frac{\lambda^2 - \frac{1}{4}}{z^2} + E \right) \Phi = 0. \quad (3.5)$$

Setting $\lambda = 1 - 2\epsilon$, this corresponds to $(\alpha_+, \alpha_-) = (1/2, \epsilon)$ and the exceptional point, where two levels merge and the Hamiltonian can be written in a Jordan block form, occurs at $\epsilon = 0$. The recursion relation (2.17) for $p_n(E, -\lambda, J)$ becomes

$$p_n = -E p_{n-1} + 16(3 - n)(n - 1)(n + 2\epsilon - 2)p_{n-2} \quad (3.6)$$

and, as expected, the second term on the RHS vanishes when $n = J + 1 = 3$. The energy eigenvalues of the two QES levels are given by the roots of $p_2(E, -\lambda, 2)$: $E_{0,1} = \pm 4i\sqrt{2\epsilon} = \pm 4\sqrt{-2\epsilon}$. The corresponding (unnormalized) eigenvectors are, from (2.15),

$$\Psi_{0,1} = z^{2\epsilon - \frac{1}{2}} \sqrt{2\epsilon} \left(1 \mp \frac{iz^2}{\sqrt{2\epsilon}} \right) e^{\frac{z^4}{4}}, \quad (3.7)$$

where $\Psi_{0,1} = \frac{\sqrt{2\epsilon}}{\Gamma(2\epsilon)} \Phi^{\text{eq.}(2.15)}|_{E_{0,1}}$. At $\epsilon = 0$ these two eigenvectors coincide, and to see the Jordan form of the Hamiltonian we proceed as in appendix A and construct

$$\begin{aligned} \phi_0 &= \Psi_0|_{\epsilon=0} = -iz^{3/2} e^{z^4/4} \\ \phi_1 &= 2a\sqrt{\epsilon} \frac{d\Psi_0}{d\epsilon} \Big|_{\epsilon=0} = a\sqrt{2} z^{-1/2} e^{z^4/4} \end{aligned} \quad (3.8)$$

where a is a constant. The Hamiltonian at $\epsilon = 0$ is

$$H_0 = -\frac{d^2}{dz^2} + z^6 + 6z^2 + \frac{3}{4z^2} \quad (3.9)$$

and requiring ϕ_0 and ϕ_1 to satisfy the ‘Jordan chain’ relations $H_0 \phi_0 = 0$ and $H_0 \phi_1 = \phi_0$ fixes $a = -\frac{i}{4\sqrt{2}}$, and shows that the Hamiltonian has the desired Jordan block form. However, this basis is not unique: replacing $\{\phi_0, \phi_1\}$ by $\{\mu\phi_0, \mu\phi_1 + \nu\phi_0\}$ preserves the Jordan chain for any constants μ and ν . This freedom can be used to make a convenient choice for our biorthogonal system. Dropping a common factor of $-i$, the general Jordan basis is

$$\phi_0 = \mu z^{3/2} e^{z^4/4} \quad (3.10)$$

$$\phi_1 = \left(\frac{1}{4}\mu z^{-1/2} + \nu z^{3/2} \right) e^{z^4/4}. \quad (3.11)$$

The integrals $\int_{i\mathbb{C}} \phi_m \phi_n dz$ with $m, n \in \{0, 1\}$ can be evaluated using (3.4) and are

$$\int_{i\mathbb{C}} \phi_0 \phi_0 dz = \mu^2 \int_{i\mathbb{C}} z^3 e^{z^4/2} dz = 0 \quad (3.12)$$

$$\int_{i\mathbb{C}} \phi_0 \phi_1 dz = \int_{i\mathbb{C}} \left(\frac{1}{4}\mu^2 z + \mu\nu z^3 \right) e^{z^4/2} dz = \frac{i\mu^2}{8} \sqrt{2\pi} \quad (3.13)$$

$$\int_{i\mathbb{C}} \phi_1 \phi_1 dz = \int_{i\mathbb{C}} \left(\frac{1}{16}\mu^2 z^{-1} - \frac{1}{2}\mu\nu z + \nu^2 z^3 \right) e^{z^4/2} dz = \frac{i\mu}{4} \left(\frac{1}{8}\pi\mu + \sqrt{2\pi}\nu \right). \quad (3.14)$$

Therefore, if

$$i\mu^2 = \frac{4\sqrt{2}}{\sqrt{\pi}}, \quad \nu = -\frac{\sqrt{\pi}}{8\sqrt{2}} \alpha \quad (3.15)$$

then $\int_{i\mathbb{C}} \phi_1 \phi_1 dz = 0$ and $\int_{i\mathbb{C}} \phi_0 \phi_1 dz = 1$, allowing us to take the dual basis to be $\tilde{\phi}_0 = \phi_1$ and $\tilde{\phi}_1 = \phi_0$.

The spectrum in the neighbourhood of H_0 can now be investigated. For this a two-parameter family of perturbations is required, and we take one of these parameters to be ϵ , and the other, η , to be orthogonal to this in the (α_+, α_-) coordinates so that $(\alpha_+, \alpha_-) = (1/2 + \eta, \epsilon)$ and

$$H = H_0 + 4(\eta + \epsilon)z^2 + 4(1 + \eta - \epsilon)(\eta - \epsilon)z^{-2}. \quad (3.16)$$

The matrix elements of interest are, in an obvious notation,

$$\langle \tilde{\phi}_{0,1} | z^2 | \phi_{0,1} \rangle = \begin{pmatrix} \frac{\sqrt{2\pi}}{4} & \frac{1}{4} - \frac{\pi}{32} \\ -4 & \frac{\sqrt{2\pi}}{4} \end{pmatrix} \quad (3.17)$$

$$\langle \tilde{\phi}_{0,1} | z^{-2} | \phi_{0,1} \rangle = \begin{pmatrix} \frac{\sqrt{2\pi}}{4} & \frac{1}{4} - \frac{3\pi}{32} \\ 4 & \frac{\sqrt{2\pi}}{4} \end{pmatrix} \quad (3.18)$$

and so the truncated Hamiltonian, to leading order, is

$$H_{pert} \approx \begin{pmatrix} 2\sqrt{2\pi}\eta & 1 \\ 16\eta^2 - 32\epsilon & 2\sqrt{2\pi}\eta \end{pmatrix}. \quad (3.19)$$

The approximate energy levels are thus the roots of the characteristic polynomial of this matrix:

$$E = 2\sqrt{2\pi}\eta \pm 4\sqrt{\eta^2 - 2\epsilon}. \quad (3.20)$$

Two special cases deserve comment. For $\eta = 0$ the QES levels $E = \pm 4\sqrt{-2\epsilon}$ are recovered, as expected given that these QES levels were used to set up the approximation scheme in the first place. More interesting is the fact that for $\epsilon = 0$ the energy levels remain real as the exceptional point is traversed. (The same phenomenon was remarked in a finite-dimensional setting in [15].) This corresponds to the fact that the approximation correctly predicts the *direction* of the line of exceptional points away from the QES point $(\alpha_+, \alpha_-) = (1/2, 0)$. However one should be wary of trusting the approximation any further – one might expect that the *curvature* of the line of exceptional points could be recovered from the line of points where the discriminant of the characteristic polynomial of (3.19) vanishes, which is $\eta^2 - 2\epsilon = 0$, or $\alpha_- = \frac{1}{2}(\frac{1}{2} - \alpha_+)^2$. However, a fit to the numerical eigenvalues of the full equation shows that the shape of the curve of exceptional points near to $(1/2, 0)$ is rather given by $\alpha_- \approx \kappa(\frac{1}{2} - \alpha_+)^2$ with $\kappa \approx 0.78$. Given that this curvature is controlled by sub-leading effects, this failure should not be too surprising, but it does highlight the delicacy of perturbation theory about exceptional points. A more systematic investigation of this issue would be valuable, but for now we will pass on to an examination of a typical cubic exceptional point.

3.2 The Jordan block at a cubic exceptional point

From table 1, the first cubic exceptional points occur at $(\alpha_+, \alpha_-) = (1, 1/4)$ and $(1/4, 1)$, on the $J = 3$ QES lines $\alpha = 12 - 2\lambda$ and $\alpha = 12 + 2\lambda$. We focus on the line $\alpha = 12 + 2\lambda$ and set $\lambda = 2\epsilon - 3/2$ so that $(\alpha_+, \alpha_-) = (\epsilon + 1/4, 1)$ and the exceptional point occurs at $\epsilon = 0$. The eigenvalue problem in terms of ϵ is

$$\left(-\frac{d^2}{dz^2} + z^6 + (4\epsilon + 9)z^2 + \frac{(2\epsilon - 1)(2\epsilon - 2)}{z^2} + E \right) \Psi = 0 \quad (3.21)$$

and the recursion relation for $p_n(E, 2\epsilon - 3/2, 3)$ is

$$p_n = -E p_{n-1} + 16(4 - n)(n - 1)(n + 2\epsilon - 5/2)p_{n-2}. \quad (3.22)$$

The roots of p_3 give the energy eigenvalues of the three QES levels: $E_0 = 0$, $E_{\pm} = \pm 8\sqrt{-2\epsilon}$. The corresponding eigenstates are

$$\begin{aligned}\Psi_0 &= e^{z^4/4} z^{2\epsilon-1} a \left(1 + \frac{2z^4}{4\epsilon+1} \right) \\ \Psi_{\pm} &= e^{z^4/4} z^{2\epsilon-1} a \left(1 \mp \frac{4\sqrt{-2\epsilon}z^2}{4\epsilon-1} - \frac{2z^4}{4\epsilon-1} \right)\end{aligned}\tag{3.23}$$

where a is some normalisation to be fixed later. Note that when $\epsilon = 0$ these three QES eigenstates merge and we have only one known eigenstate at this point, namely

$$\Psi_0|_{\epsilon=0} = a e^{z^4/4} \left(\frac{1}{z} + 2z^3 \right).\tag{3.24}$$

3.2.1 The Jordan basis

If we perturb away from the cubic exceptional point along the QES line, the Hamiltonian will correspond to a toy model matrix of the form

$$L(\epsilon) = \begin{pmatrix} 0 & 1 & 0 \\ \epsilon/2 & 0 & 1 \\ 0 & \epsilon/2 & 0 \end{pmatrix}.\tag{3.25}$$

The method that we used to calculate the Jordan basis for the quadratic exceptional point in section 3.1, explained for $n \times n$ Jordan blocks in appendix A, does not apply here. This is because the matrix considered in appendix A would correspond to a perturbation of the Hamiltonian along a line perpendicular to the QES line, along which we do not know the relevant eigenfunctions analytically. Instead, we will have to find the basis functions for (3.25) by solving the Jordan chain constraints directly, to find wavefunctions ϕ_0 , ϕ_1 and ϕ_2 that satisfy

$$\begin{aligned}H_0\phi_0 &= 0 \\ H_0\phi_1 &= \phi_0 \\ H_0\phi_2 &= \phi_1\end{aligned}\tag{3.26}$$

where H_0 is the Hamiltonian at the cubic exceptional point:

$$H_0 = -\frac{d^2}{dz^2} + z^6 + 9z^2 + \frac{2}{z^2}.\tag{3.27}$$

Note that $H_0 \Psi_0|_{\epsilon=0} = 0$ so we can take $\phi_0 = \Psi_0|_{\epsilon=0}$. Then solving (3.26) for ϕ_1 and ϕ_2 , we find

$$\begin{aligned}\phi_1 &= e^{z^4/4} \left(\frac{az}{2} + b \left(\frac{1}{z} + 2z^3 \right) \right) \\ \phi_2 &= e^{z^4/4} \left(\frac{a}{16z} + \frac{bz}{2} + c \left(\frac{1}{z} + 2z^3 \right) \right)\end{aligned}\tag{3.28}$$

with a , b and c constants, arbitrary at this stage. These are the most general solutions to (3.26) that also satisfy the relevant boundary condition, that is square integrability along $i\mathcal{C}$.

Now that we have a basis, we must find the dual basis $\tilde{\phi}_0$, $\tilde{\phi}_1$ and $\tilde{\phi}_2$ which satisfies

$$\begin{aligned}\int_{i\mathcal{C}} \phi_i \tilde{\phi}_i dz &= 1, \text{ for } i = 0, 1, 2 \\ \int_{i\mathcal{C}} \phi_i \tilde{\phi}_j dz &= 0, \text{ for } i \neq j.\end{aligned}\tag{3.29}$$

From [16] we expect the dual basis to be $\tilde{\phi}_0 = \phi_2$, $\tilde{\phi}_1 = \phi_1$ and $\tilde{\phi}_2 = \phi_0$ and this is supported by the fact that $\int_{i\mathcal{C}} \phi_0 \phi_0 dz = \int_{i\mathcal{C}} \phi_0 \phi_1 dz = 0$ and $\int_{i\mathcal{C}} \phi_1 \phi_1 dz \propto a^2$. Fixing $\int_{i\mathcal{C}} \phi_2 \phi_2 dz = 0$ and $\int_{i\mathcal{C}} \phi_1 \phi_2 dz = 0$ constrains the coefficients b and c to be

$$\begin{aligned} b &= -\frac{a\pi}{16\Gamma(3/4)^2} \\ c &= \frac{a(3\pi^2 - 8\Gamma(3/4)^4)}{512\Gamma(3/4)^4}. \end{aligned} \quad (3.30)$$

Then requiring $\int_{i\mathcal{C}} \phi_1 \phi_1 dz = \int_{i\mathcal{C}} \phi_0 \phi_2 dz = 1$ fixes a^2 :

$$a^2 = -\frac{2^{11/4}i}{\Gamma(3/4)}. \quad (3.31)$$

Choosing the root with positive real part for a we have fixed the basis to be

$$\begin{aligned} \phi_0 &= \frac{(1-i)2^{7/8}}{\sqrt{\Gamma(\frac{3}{4})}} e^{z^4/4} \left(\frac{1}{z} + 2z^3 \right) \\ \phi_1 &= \frac{(i-1)2^{7/8}}{16\Gamma(\frac{3}{4})^{5/2}} e^{z^4/4} \left(\frac{\pi}{z} - 8z\Gamma\left(\frac{3}{4}\right)^2 + 2\pi z^3 \right) \\ \phi_2 &= \frac{(1-i)2^{7/8}}{512\Gamma(\frac{3}{4})^{9/2}} e^{z^4/4} \left(\frac{24\Gamma(\frac{3}{4})^4 + 3\pi^2}{z} - 16\pi\Gamma\left(\frac{3}{4}\right)^2 z + 6\pi^2 z^3 - 16\Gamma\left(\frac{3}{4}\right)^4 z^3 \right) \end{aligned} \quad (3.32)$$

with the dual basis $\tilde{\phi}_0 = \phi_2$, $\tilde{\phi}_1 = \phi_1$ and $\tilde{\phi}_2 = \phi_0$.

3.2.2 Matrix elements and the cusp singularity

We first perturb away from the cusp along the QES line $(\alpha_+, \alpha_-) = (\epsilon + 1/4, 1)$ and write

$$H = H_0 + V, \quad (3.33)$$

where $V = \frac{4\epsilon^2 - 6\epsilon}{z^2} + 4\epsilon z^2$ is considered as a perturbation of H_0 (3.27). The required matrix elements are

$$\langle \tilde{\phi}_2 | V | \phi_0 \rangle = \frac{128\pi\epsilon^2}{3\Gamma(\frac{3}{4})^2}, \quad (3.34)$$

and

$$\begin{aligned} \langle \tilde{\phi}_1 | V | \phi_0 \rangle &= \langle \tilde{\phi}_2 | V | \phi_1 \rangle \\ &= -\frac{8\epsilon}{3\Gamma(\frac{3}{4})^4} \left(24\Gamma\left(\frac{3}{4}\right)^4 - 12\Gamma\left(\frac{3}{4}\right)^4 \epsilon + \pi^2 \epsilon \right) \\ &\approx -64\epsilon \end{aligned} \quad (3.35)$$

to leading order in ϵ . To investigate the shape of the cusp we also need to perturb away from the exceptional point in the direction perpendicular to the QES line, i.e. along η where $\alpha = -4\eta + 9$ and $\lambda = 2\eta - 3/2$, or $\alpha_+ = 1/4$ and $\alpha_- = 1 - \eta$. The Hamiltonian is now $H = H_0 + V + V'$ with

$$V' = -4\eta z^2 + \frac{2\eta(2\eta - 3)}{z^2}, \quad (3.36)$$

and to first order in η we find

$$\langle \tilde{\phi}_2 | V' | \phi_0 \rangle = \frac{128\eta\pi(\eta - 3)}{3\Gamma(\frac{3}{4})^2} \approx -\frac{128\pi\eta}{\Gamma(\frac{3}{4})^2}. \quad (3.37)$$

The remaining matrix elements effect the energy levels only at subleading order in η and so they can consistently be ignored. The resulting truncated Hamiltonian is

$$H_{pert} \approx \begin{pmatrix} 0 & 1 & 0 \\ -64\epsilon & 0 & 1 \\ -\frac{128\pi\eta}{\Gamma(3/4)^2} & -64\epsilon & 0 \end{pmatrix}. \quad (3.38)$$

The matrix (3.38) has the characteristic polynomial $X^3 + 128\epsilon X + \frac{128\pi\eta}{\Gamma(3/4)^2} = 0$. Now the curve of exceptional points occurs when $dX/d\epsilon \rightarrow \infty$ (or equivalently $dX/d\eta \rightarrow \infty$). Since

$$\frac{dX}{d\epsilon} = \frac{-128X}{3X^2 + 128\epsilon} \quad (3.39)$$

the requirement $dX/d\epsilon \rightarrow \infty$ fixes

$$X = \pm \sqrt{-\frac{128\epsilon}{3}}. \quad (3.40)$$

Substituting this into the characteristic polynomial above and restricting to $\epsilon \leq 0$ gives the following relation between η and ϵ :

$$\eta = \pm \frac{2}{3} \sqrt{\frac{128}{3} \frac{\Gamma(3/4)^2}{\pi}} |\epsilon|^{3/2}. \quad (3.41)$$

For $\epsilon > 0$ the relation (3.40) is not real indicating that there are no exceptional points in this region, which matches our numerical results. In terms of the α_{\pm} notation, $\alpha_+ = \epsilon + 1/4$ and $\alpha_- = 1 - \eta$ so this relation becomes:

$$\alpha_- = 1 \pm \frac{2}{3} \sqrt{\frac{128}{3} \frac{\Gamma(3/4)^2}{\pi}} (1/4 - \alpha_+)^{3/2} \quad (3.42)$$

which is valid for α_- close to 1 and $0 \ll \alpha_+ \leq 1/4$.

A comparison between the prediction (3.42) for the line of exceptional points in the vicinity of the cusp at $(\alpha_+, \alpha_-) = (1/4, 1)$ and numerical data obtained from a direct solution of the eigenvalue problem is shown in figure 12. The shape of the curve is accurately reproduced. In principle the same calculations could be performed for other cusps, though the relevant wavefunctions become more complicated.

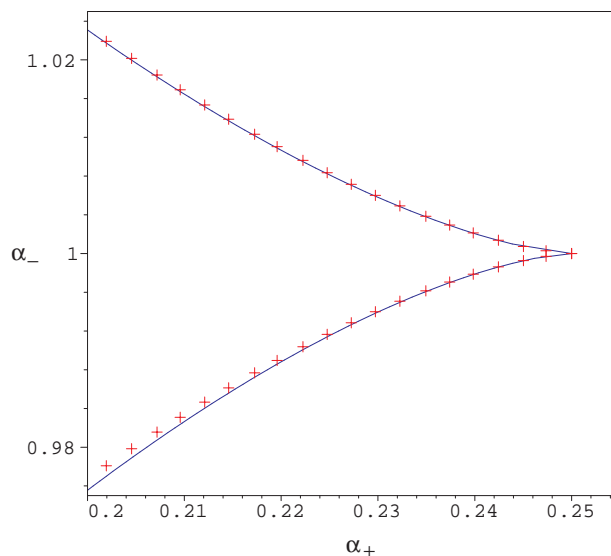


Figure 12: The first cusp for $M = 3$: the crosses show the prediction (3.42) while the solid line was found by solving the full problem.

4 Numerical results for $M \neq 3$

Having established the existence of quadratic and cubic exceptional points at $M = 3$, we now explore the situation at other values of M . Whitney's theorem for mappings from the plane to the plane [24] implies that the fold and cusp singularities (corresponding to the doubly-exceptional lines and triply-exceptional cusp points seen at $M = 3$) are stable, and so the pattern of cusped lines must persist, at least while M remains sufficiently close to 3. Recall also that protected zero-energy levels lie on the lines $\alpha_{\pm} = n$ for all values of M . However, away from $M = 3$ quasi-exact solvability is lost, and so one of the properties which confined the cusps at $M = 3$ to the lines $\alpha_{\pm} = n$, namely the symmetry of the set of merging levels under $E \rightarrow -E$, may no longer hold.

Figures 13, 14 and 15 show the exceptional lines for $M = 2$, 1.5 and 1.3. The plots were obtained by a direct numerical solution of the second dual form of the eigenvalue problem, as described in appendix B.

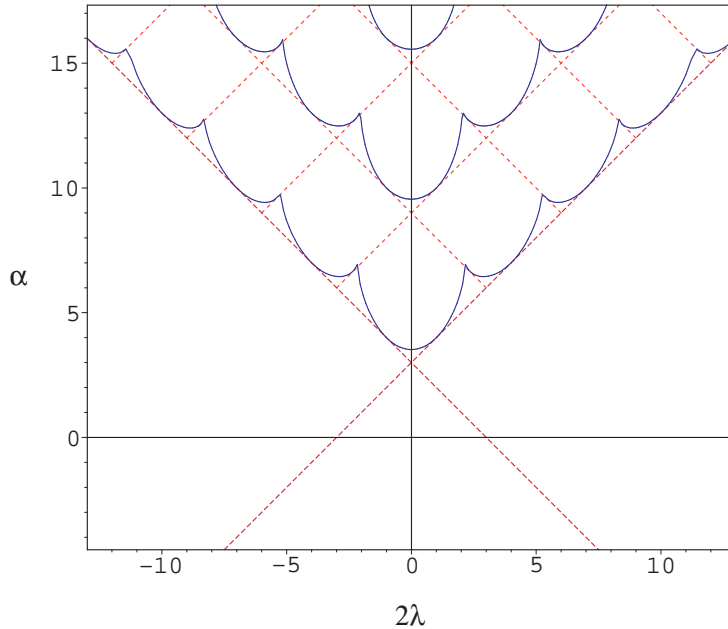


Figure 13: Exceptional lines at $M = 2$.

As predicted, the overall pattern remains the same, but the cusps move away from the protected zero-energy lines. The points where the outermost cusped line touches the supersymmetric zero-energy lines $\alpha_{\pm} = 0$ are known exactly, from (2.2). As M decreases from 3, they move down from the midpoints between $\alpha_{\mp} = n$ and $\alpha_{\mp} = n + 1$ along the lines $\alpha_{\pm} = 0$, as predicted by the formula (2.13). At the same time, the numerical data shows that the cusps move upwards, on the rescaled coordinates of the plots which keep the lines of protected zero-energy levels at constant locations. As $M \rightarrow 1^+$ the pattern shows signs of simplifying, with the cusps heading away towards $\alpha = +\infty$ and the regions of unreality shrinking towards the lines $2\lambda \in 2\mathbb{Z}$. This behaviour will be discussed further in section 5.

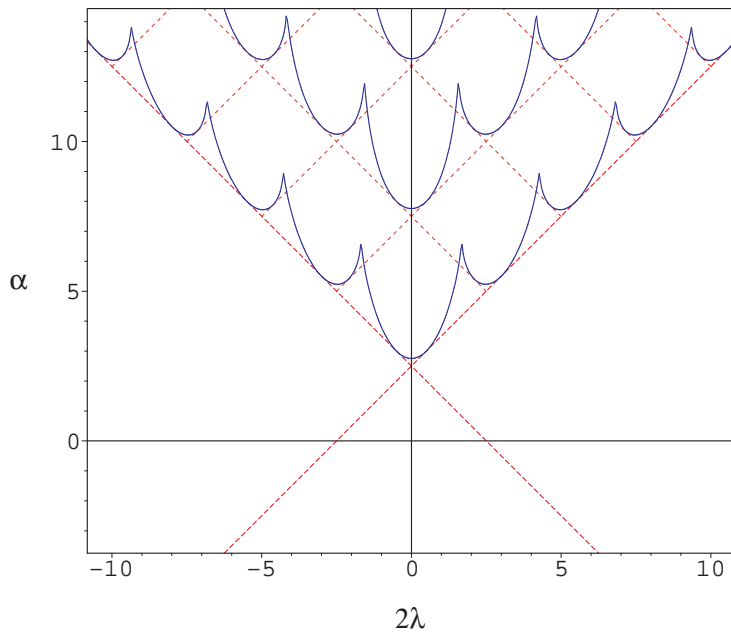


Figure 14: Exceptional lines at $M = 1.5$.

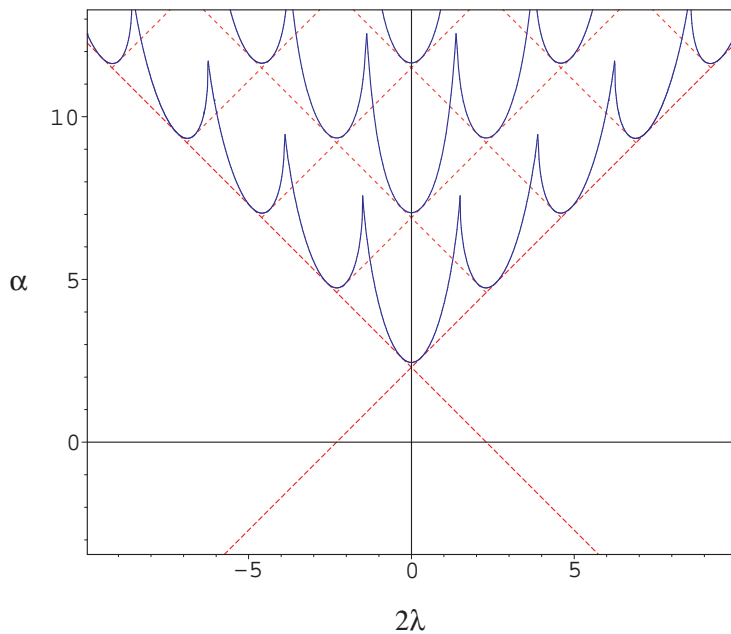


Figure 15: Exceptional lines at $M = 1.3$.

It is interesting to see the fate of the exceptional points corresponding to the zeros of the polynomials $Q_n(\lambda)$, which at $M = 3$ are triply-exceptional cusps. For $M \neq 3$ the cusps move away from the lines $\alpha_{\pm} \in \mathbb{N}$, and so the zeros of the $Q_n(\lambda)$ are no longer cusps, but are instead only doubly exceptional. Furthermore, the presence of an exactly-zero level on the lines $\alpha_{\pm} \in \mathbb{N}$ forces the smooth parts of the exceptional lines to be tangent to these lines immediately M moves away from 3, and this leads to a complicated change in the shape of these curves, illustrated in figure 16.

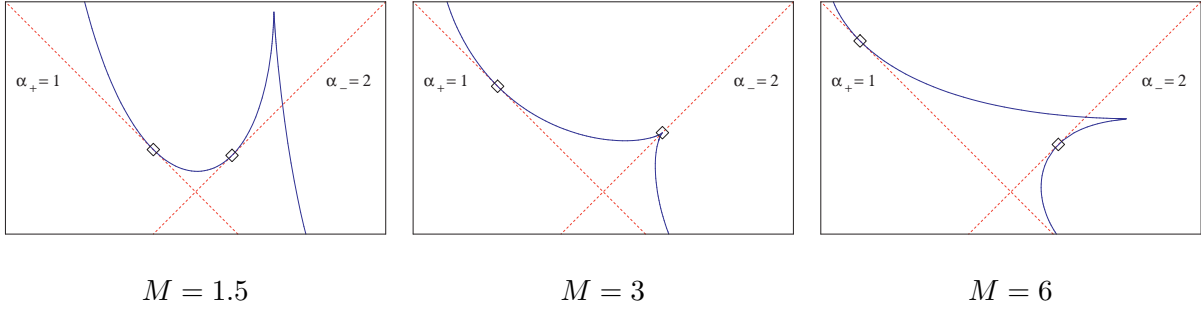


Figure 16: The movement of a cusp for $M \neq 3$.

The plots of figure 16 indicate that for $M > 3$ the movement of the cusps away from the lines $\alpha_{\pm} \in \mathbb{N}$ is opposite to that for $M < 3$, and this can also be seen in figures 17 and 18, which show the exceptional lines for $M = 10$ and $M = 30$. Again, the locations of the zero-energy exceptional points on the lines α_{\pm} confirm the formula (2.13), and there are no hints of any further exceptional points beyond those predicted by our general considerations. As the cusps move towards the α axis, they start to merge to leave isolated ‘islands’ of unreality in the phase diagram. In the theory of singularities, this merging of two cusps is sometimes called the ‘beaks’ transition (see, for example, [25] and references therein). As for $M \rightarrow 1^+$, the structure simplifies as $M \rightarrow \infty$.

It turns out that the simplifications near to $M = 1$ and $M = \infty$ can be understood analytically, using the fact that the limiting points $M = 1$ and $M = \infty$ are exactly solvable, and allow perturbative treatments to be set up in their vicinities. In the next two sections this will be developed in detail, starting with the region near to $M = 1$ where we will see that it leads to a novel insight into the original ‘Bender-Boettcher’ phase transition to infinitely-many complex levels, which occurs when M becomes smaller than 1.

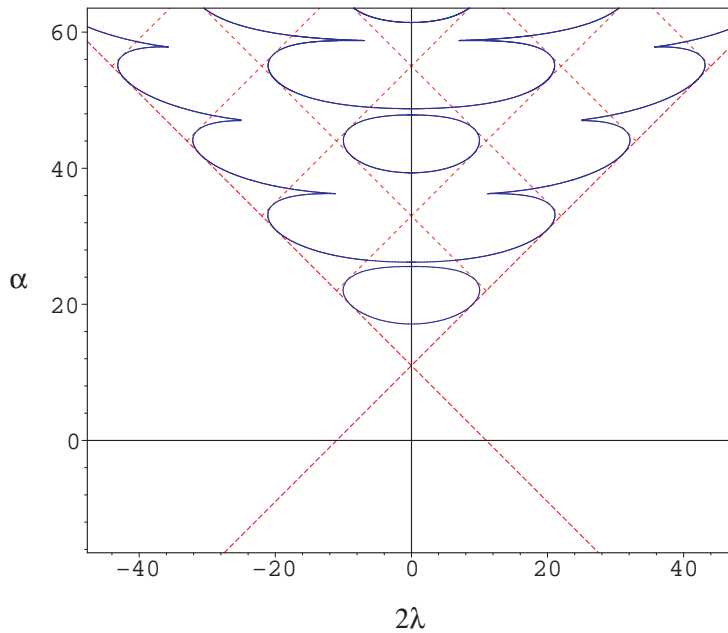


Figure 17: Exceptional lines at $M = 10$.

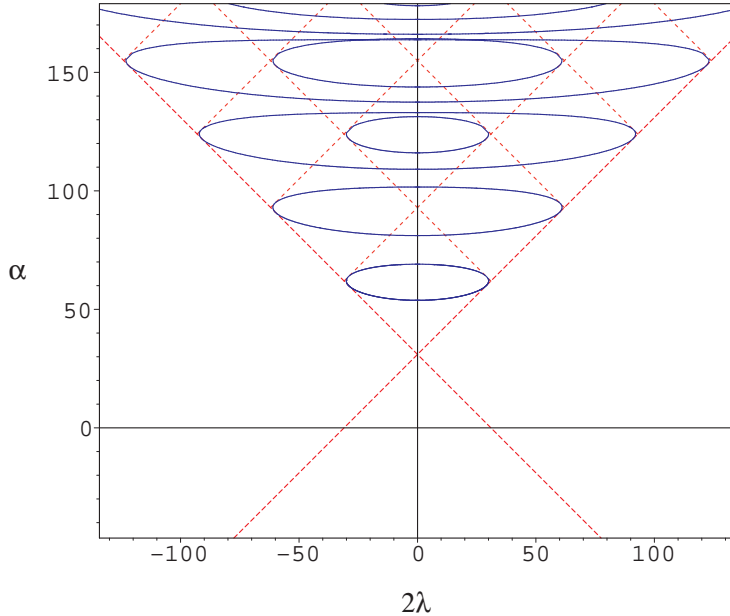


Figure 15: Exceptional lines at $M = 30$.

5 Perturbation theory about $M = 1$

5.1 Exceptional points via near-degenerate perturbation theory

In this section we revert to the original formulation of the eigenvalue problem, namely

$$H_M \psi(x) = E \psi(x), \quad \psi(x) \in L^2(\mathcal{C}) \quad (5.1)$$

where

$$H_M = -\frac{d^2}{dx^2} - (ix)^{2M} - \alpha(ix)^{M-1} + \frac{\lambda^2 - \frac{1}{4}}{x^2}. \quad (5.2)$$

For $M = 1$ this problem can be solved exactly – it is the \mathcal{PT} -symmetric simple harmonic oscillator [11, 26], and its spectrum is entirely real. (Note, for $\lambda^2 - \frac{1}{4} \neq 0$ the wavefunctions themselves can be complex, owing to the singularity of the potential at the origin and the departure of the quantisation contour from the real axis there.) As M moves away from 1, pairs of eigenvalues can become complex; as discussed earlier, this is always preceded by the coincidence of two real eigenvalues and so the first complex eigenvalues will emerge from points in the $(2\lambda, \alpha)$ plane at which the spectrum has degeneracies for $M = 1$. We aim to investigate exactly how this occurs.

In [27], Bender *et al.* used a perturbative approach to study the spectrum for M near 1 with $\alpha = 0$ and $\lambda^2 = \frac{1}{4}$. The full Hilbert space was truncated to the subspace spanned by $M = 1$ eigenfunctions $|2n-1\rangle$ and $|2n\rangle$, where $H_1|m\rangle = (2m+1)|m\rangle$, $m \in \mathbb{Z}^+$, and H_M expanded within that two-dimensional subspace about $H_{M=1}$. Diagonalising the resulting 2×2 matrix yielded an approximation to the eigenvalues of H_M . However, as shown in [28], this approximation predicts level-merging for both signs of $M-1$ rather than the one sign actually observed, and when applied to the pair of levels $|2n\rangle$ and $|2n+1\rangle$, it predicts that they too will merge, contrary to the actual behaviour of the model. These problems can be traced to the fact that the $M = 1$ eigenvalues at $\alpha = \lambda^2 - \frac{1}{4} = 0$ are equally spaced, making the truncation to the subspace spanned by $|2n-1\rangle$ and $|2n\rangle$ unjustified.

For the more general Hamiltonian (5.2) the situation can be improved, as α and λ can be tuned so as to make some pairs of levels close to each other relative to all of the others. Truncation

to these levels will then be reliable, and as we show below it gives a good approximation to their behaviour for M close to 1.

To see how a consistent prediction of exceptional points can emerge from this approach, it is worth examining a simple 2×2 example which illustrates the main features. Consider the ‘unperturbed’ Hamiltonian

$$H_1(\eta) = \begin{pmatrix} 2\eta & 0 \\ 0 & -2\eta \end{pmatrix} \quad (5.3)$$

where η will be considered small but fixed, with the eigenvalues $\pm 2\eta$ corresponding to the nearby pair of energies in the full problem. Add to it a perturbation with both diagonal and off-diagonal parts:

$$V_\epsilon(\eta) = -\frac{\epsilon}{\eta} \begin{pmatrix} \alpha & i \\ i & -\alpha \end{pmatrix} \quad (5.4)$$

where α is fixed and ϵ is the perturbing parameter (corresponding to $M - 1$ in the full problem). The factor of $1/\eta$ will reflect the fact that nearby levels in the unperturbed problem interact more strongly as they approach each other. Then $H_{1+\epsilon} = H_1 + V_\epsilon$ has eigenvalues

$$E_\pm = \pm \sqrt{(2\eta - \alpha\epsilon/\eta)^2 - \epsilon^2/\eta^2} \quad (5.5)$$

and exceptional points at $\epsilon = \pm \frac{2}{1 \pm \alpha} \eta^2$. For fixed $\alpha \neq \pm 1$ the two exceptional points are at $\epsilon = O(\eta^2)$, so, even with the $1/\eta$ factor in its specification, $V_\epsilon(\eta)$ is still small at their locations. For $\alpha = \pm 1$ one exceptional point is pushed away to infinity, but the other remains in a region where the perturbation is still small.

5.2 Perturbative locations of the exceptional points

Returning to the original problem, the Hamiltonian at $M = 1$ is

$$H_1 = -\frac{d^2}{dx^2} + x^2 + \frac{\lambda^2 - \frac{1}{4}}{x^2} - \alpha. \quad (5.6)$$

With the given boundary conditions, H_1 has c -normalised eigenfunctions [29]

$$\phi_n^\pm(x) = \frac{\sqrt{2}\sqrt{n!}}{\sqrt{(1 - e^{\mp 2\pi i \lambda})\Gamma(\pm \lambda + n + 1)}} x^{1/2 \pm \lambda} e^{-\frac{x^2}{2}} L_n^{\pm \lambda}(x^2), \quad n = 0, 1, \dots \quad (5.7)$$

where the L_n^β are Laguerre polynomials. The corresponding eigenvalues are

$$E_n^\pm = -\alpha + 4n + 2 \pm 2\lambda. \quad (5.8)$$

A degenerate eigenvalue occurs when $E_n^+ = E_m^-$ for some n and m , which requires

$$\lambda = m - n. \quad (5.9)$$

Thus, on the vertical lines $2\lambda \in 2\mathbb{Z}$ in the $(2\lambda, \alpha)$ plane, infinitely-many pairs of the eigenfunctions (5.7) are proportional to each other. Indeed, if $\lambda = q$ is a non-negative integer, then for all non-negative integers p , $\phi_{p+q}^- = i(-1)^q \phi_p^+$. Since $\phi_n^+ \rightarrow \phi_n^-$ when $\lambda \rightarrow -\lambda$, it also follows that $\phi_{p+q}^+ \propto \phi_p^-$ when $\lambda = -q$.

In order to find the eigenvalues of H_M for $M = 1 + \epsilon$, we treat $H_M = H_{1+\epsilon}$ in a basis of near-degenerate eigenfunctions of H_1 by writing it as

$$H_{1+\epsilon} = H_1 + V_\epsilon \quad (5.10)$$

where H_1 is given by (5.6) and

$$V_\epsilon = -x^2 - (ix)^{2+2\epsilon} - \alpha(ix)^\epsilon. \quad (5.11)$$

The exact matrix elements of V_ϵ in the truncated basis of H_1 eigenfunctions were found by Millican-Slater [29], and are reproduced in appendix C, while those of H_1 are given by (5.8). Rediagonalising the resulting 2×2 matrix gives the approximate energy levels.

To find the exceptional points reliably, we require both that the perturbation is small, and that the two levels in the truncated subspace are close. With $M = 1 + \epsilon$ and $\lambda = q + \eta$, this means that ϵ and η must be small. In fact, we shall see that the exceptional points occur when ϵ is of order η^2 , and our approximations will be good in this region. We shall also assume that $q \geq 0$, as results for negative q are easily restored using the $\lambda \rightarrow -\lambda$ symmetry of the problem. For small values of η , the pairs of levels $\{\phi_p^+, \phi_{p+q}^-\}$, $p \geq 0$, are almost degenerate; to lighten the notation, we fix the integer $p \geq 0$ and denote the corresponding basis by $\{\phi^+, \phi^-\} \equiv \{\phi_p^+, \phi_{p+q}^-\}$. The matrix elements of H_1 are

$$\langle \phi^+ | H_1 | \phi^+ \rangle = 4p + 2q + 2\eta + 2 \quad (5.12)$$

$$\langle \phi^- | H_1 | \phi^- \rangle = 4p + 2q - 2\eta + 2 \quad (5.13)$$

$$\langle \phi^+ | H_1 | \phi^- \rangle = \langle \phi^- | H_1 | \phi^+ \rangle = 0, \quad (5.14)$$

while those of V_ϵ follow from (C.2), (C.3) and (C.5).

Expanding in ϵ and η and retaining terms proportional to η , ϵ/η , ϵ and ϵ^2/η the matrix elements $H_{ab} \equiv \langle \phi^a | H_M | \phi^b \rangle$ are

$$\begin{aligned} H_{++} &\approx 4p + 2q + 2 - \alpha + \left(2p + q + 1 - \frac{\alpha}{2}\right) \frac{\epsilon}{\eta} + 2\eta \\ &\quad + \left(\left(2p + q + 1 - \frac{\alpha}{2}\right) \psi(p + q + 1) + 2p + 2\right) \epsilon \\ &\quad + \left(\left(2p + q + 1 - \frac{\alpha}{4}\right) \psi(p + q + 1) + 2p + 1\right) \frac{\epsilon^2}{\eta}; \end{aligned} \quad (5.15)$$

$$\begin{aligned} H_{--} &\approx 4p + 2q + 2 - \alpha - \left(2p + q + 1 - \frac{\alpha}{2}\right) \frac{\epsilon}{\eta} - 2\eta \\ &\quad + \left(\left(2p + q + 1 - \frac{\alpha}{2}\right) \psi(p + 1) + 2p + 2q + 2\right) \epsilon \\ &\quad - \left(\left(2p + q + 1 - \frac{\alpha}{4}\right) \psi(p + q + 1) + 2p + 1\right) \frac{\epsilon^2}{\eta}; \end{aligned} \quad (5.16)$$

$$\begin{aligned} H_{+-} &\approx \frac{i}{|\eta|} \left[\left(2p + q + 1 - \frac{\alpha}{2}\right) \epsilon \right. \\ &\quad + \left. \left(\frac{1}{2} \left(2p + q + 1 - \frac{\alpha}{2}\right) (\psi(p + q + 1) - \psi(p + 1)) - q\right) \epsilon \eta \right. \\ &\quad + \left. \left(\left(2p + q + 1 - \frac{\alpha}{4}\right) \psi(p + q + 1) + 2p + 1\right) \epsilon^2 \right] \end{aligned} \quad (5.17)$$

where $\psi(z) = \Gamma'(z)/\Gamma(z)$. Diagonalising H_{ab} , the approximate eigenvalues E_\pm at $M = 1 + \epsilon$, $\lambda = q + \eta$, α are:

$$\begin{aligned} E_\pm &= 4p + 2q + 2 - \alpha + \left(2p + q + 2 + \frac{1}{4}(4p + 2q + 2 - \alpha)(\psi(p + q + 1) + \psi(p + 1))\right) \epsilon \\ &\quad \pm \left[(8p + 4q + 4 - 2\alpha)\epsilon + 4\eta^2 \right. \\ &\quad + \left. \left((4p + 2q + 2 - \alpha)(\psi(p + q + 1) - \psi(p + 1)) - 4q \right) \epsilon \eta \right. \\ &\quad + \left. \left. \left((8p + 4q + 4 - \alpha)\psi(p + q + 1) + 8p + 4 \right) \epsilon^2 \right]^{1/2}. \end{aligned} \quad (5.18)$$

Within this approximation, exceptional points occur on the curves on the $(2\lambda, \alpha)$ plane where the argument of the square root in (5.18) vanishes. These curves, and their images under $\lambda \rightarrow -\lambda$,

are plotted in figures 19 and 20 for $\epsilon = 0.005$ and $\epsilon = 0.02$ respectively. Each shows the exceptional lines corresponding to p and q equal to 0, 1 and 2. (The exceptional lines for other values of p and q are outside the regions shown on the plots.) The dotted lines indicate $\alpha_{\pm} \in \mathbb{Z}^+$, as previously.

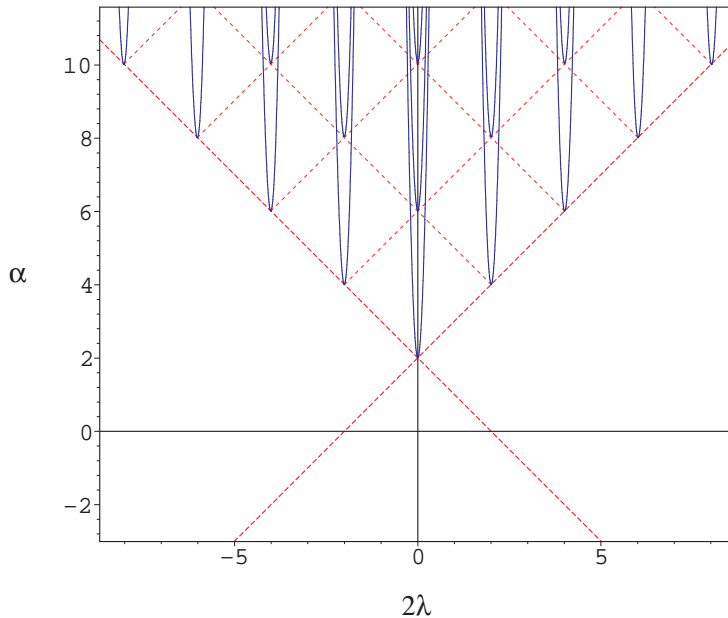


Figure 19: Perturbative lines of exceptional points for $M = 1.005$.

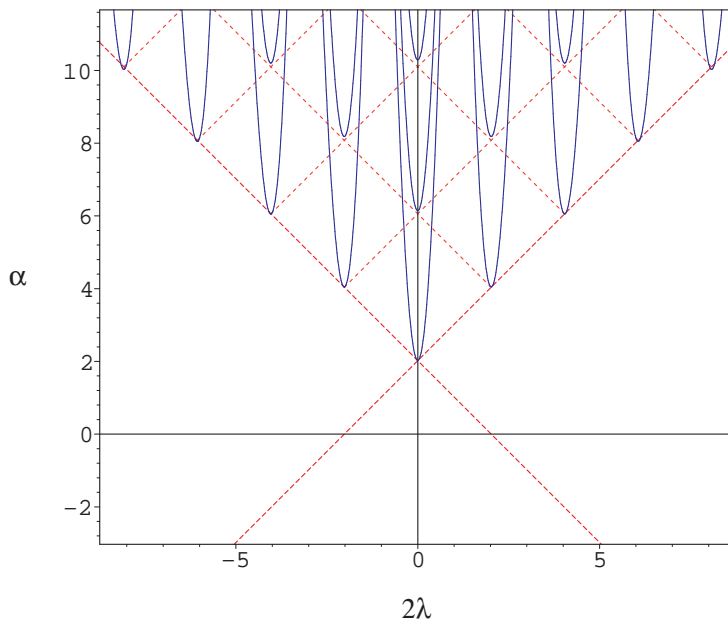


Figure 20: Perturbative lines of exceptional points for $M = 1.02$.

As M increases, regions of complex eigenvalues open up from the lines $\lambda \in \mathbb{Z}$, starting near the bottom of the spectrum. While the mergings of these regions and the joinings of their exceptional lines to form cusps cannot be seen within this approximation (since the truncation is to just two levels), the pictures are consistent with the numerical evidence in the last section that the cusps move down from $\alpha = +\infty$ as M increases from 1 towards 3.

The clearest insight into the transitions near $M = 1$ comes on retaining only the leading terms of the matrix elements for small η and ϵ , namely those proportional to η and ϵ/η . For $\lambda = q + \eta$ and $M = 1 + \epsilon$ as before, the matrix elements in the basis $\{\phi^+, \phi^-\} = \{\phi_p^+, \phi_{p+q}^-\}$ simplify to

$$\begin{pmatrix} H_{++} & H_{+-} \\ H_{-+} & H_{--} \end{pmatrix} \approx \begin{pmatrix} -2\kappa & 0 \\ 0 & -2\kappa \end{pmatrix} + \begin{pmatrix} 2\eta & 0 \\ 0 & -2\eta \end{pmatrix} + \begin{pmatrix} -\kappa\epsilon/\eta & -i\kappa\epsilon/\eta \\ -i\kappa\epsilon/\eta & \kappa\epsilon/\eta \end{pmatrix} \quad (5.19)$$

where

$$\kappa = \frac{1}{2}\alpha - 2p - q - 1. \quad (5.20)$$

The approximate eigenvalues are then

$$E_{approx} = -2\kappa \pm 2\sqrt{\eta^2 - \kappa\epsilon}. \quad (5.21)$$

Apart from the overall shift by -2κ and the replacement of ϵ by $\kappa\epsilon$, (5.19) and (5.21) have exactly the same form as the toy example (5.5) at $\alpha = 1$, one of the two values for which an exceptional point is found for only one sign of ϵ . Thus our approximation captures an important feature of the full problem which was missed by the simpler approach used in [27]. Exceptional points occur when the argument of the square root in (5.21) vanishes. At fixed ϵ , and using the $\lambda \rightarrow -\lambda$ symmetry, this happens on the parabolas

$$\alpha = 4p + 2q + 2 + \frac{1}{2\epsilon}(2\lambda \pm 2q)^2 \quad (5.22)$$

on the $(2\lambda, \alpha)$ plane, where p and q are non-negative integers. Thus there is a parabola rooted at every intersection of the lines $\alpha^+ \in \mathbb{Z}^+$, $\alpha^- \in \mathbb{Z}^+$. However, there is a significant difference between the situations for $\epsilon > 0$ ($M > 1$) and for $\epsilon < 0$ ($M < 1$). For $\epsilon > 0$, the parabolas are upwards convex, as in figures 19 and 20 above. Any fixed value of λ and α in the neighbourhood of a line $\lambda = q$ within which the 2×2 truncations are valid lies inside only finitely many of the parabolas centred on that line, and thus sees only finitely many complex eigenvalues.

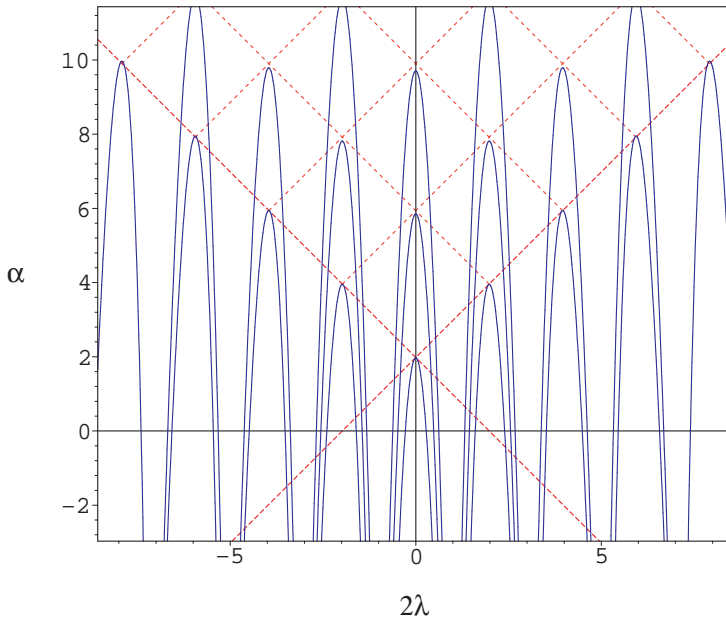


Figure 21: Perturbative lines of exceptional points for $M = 0.98$, with only a subset of the lines shown.

By contrast, for $\epsilon < 0$ the parabolas are oppositely-oriented, as in figure 21. Any given point $(2\lambda, \alpha)$ near to a line $\lambda = q$ now lies inside infinitely many of the parabolas centred on

that line, and outside only a finite number of them. Thus truncation predicts that infinitely-many eigenvalues will be complex, with only finitely many remaining real, these real levels lying at the bottom of the spectrum. This is exactly as is observed in the full problem. The transition to infinitely-many complex eigenvalues was first noted by Bender and Boettcher [3] for $\lambda = 1/2$, $\alpha = 0$. It was subsequently treated analytically, for general λ though still with $\alpha = 0$, in [28], using a non-linear integral equation for the eigenvalues found via the Bethe Ansatz approach to the problem. While the latter approach is more systematic, the perturbative understanding of the phase transition just given is particularly transparent, and gives a more immediate understanding of the regions in the $(2\lambda, \alpha)$ plane where complex levels are first to be found.

A check on the truncation method can be made using the asymptotic obtained in [28] for the value of $M = M_{\text{crit}} < 1$ at which high-lying eigenvalues E merge. With $M_{\text{crit}} = 1 + \epsilon_{\text{crit}}$ and $\lambda \neq 1/2$, this is[‡]:

$$\epsilon_{\text{crit}} \sim \frac{4 \ln |\cos(\pi\lambda)|}{\pi^2 E}. \quad (5.23)$$

For $\lambda = q + \eta$ and η small, this implies $\epsilon_{\text{crit}} \sim -2\eta^2/E$. This is easily seen to match the result just obtained, since (5.21) places the exceptional points at $\epsilon = \eta^2/\kappa$, and for E large, $E \sim -2\kappa$.

In table 2 the various approximations used in this section are compared with numerical data obtained from a direct solution of the ordinary differential equation. The numerical eigenvalues found by solving the full problem are denoted by E_{exact} ; their numerical errors are smaller than the last quoted digit. The result using the 2×2 truncation and the exact matrix elements is E_{trunc} , the initial approximated truncation (including the terms proportional to ϵ and ϵ^2/η) is E_{\pm} , and the final approximation (retaining only terms proportional to η and ϵ/η in the matrix elements) is E_{approx} . The table shows the comparison for sample values of ϵ , α and η , for for $p = q = 0$ (i.e. $\lambda = \eta$) and $p = 0, q = 1$ (i.e. $\lambda = 1 + \eta$).

$p = q = 0$				
	$\epsilon = 0.001, \alpha = 0.9, \eta = 0.01$		$\epsilon = 0.001, \alpha = 0.9, \eta = 0.25$	
E_{exact}	1.05069482	1.15266823	0.599733995	1.60332810
E_{trunc}	1.05069431	1.15266441	0.599733083	1.60332370
E_{\pm}	1.05067066	1.15269439	0.599485149	1.60387991
E_{approx}	1.04900980	1.15099019	0.597804819	1.60219518
$p = 0, q = 1$				
	$\epsilon = 0.01, \alpha = 3.9, \eta = 0.01$		$\epsilon = 0.01, \alpha = 3.9, \eta = 0.25$	
E_{exact}	0.07899348	0.18089945	-0.36215520	0.62170890
E_{trunc}	0.07897778	0.18034086	-0.36225580	0.62111404
E_{\pm}	0.07913480	0.18078797	-0.36280969	0.62273248
E_{approx}	0.05101020	0.14898979	-0.40199601	0.60199601

Table 2: Comparison of the various approximation methods used for $M \approx 1$.

The treatment so far has concerned the limiting region $|\epsilon| \ll \eta \ll 1$, which suffices to capture the behaviour of the exceptional lines as $\eta \rightarrow 0$. Other limits are also interesting, and in closing this section we remark that other presentations of the Hamiltonian may then be useful. As an example, we return to the toy model (5.3), (5.4), at $\alpha = 1$, and consider taking $\eta \rightarrow 0$ *before*

[‡]When comparing with eq.(5.37) of [28], note that the ϵ used there is equal to $2M - 2$, and not $M - 1$.

$\epsilon \rightarrow 0$. As in [17], one can introduce a pair of matrices

$$P = \frac{1}{\sqrt{2}} \begin{pmatrix} 1 & i \\ i & 1 \end{pmatrix}, \quad R = \begin{pmatrix} q & 0 \\ 0 & 1/q \end{pmatrix} \quad (5.24)$$

where $q^2 = 2i\epsilon/\eta$. Then $H_{1+\epsilon} = H_1 + V_\epsilon$ is similar to

$$\widehat{H}_{1+\epsilon} = R^{-1}P^{-1}H_{1+\epsilon}PR = \begin{pmatrix} 0 & 1 + \eta^2/\epsilon \\ 4\epsilon & 0 \end{pmatrix}. \quad (5.25)$$

It is now possible to set $\eta = 0$, showing that the Jordan block is indeed recovered as the limit is taken.

6 Perturbation theory about $M = \infty$

In this section we complete our analysis with a perturbative study about the model at $M = \infty$, which is shown in appendix D to be exactly solvable. For large M , the second duality of appendix B maps the original eigenproblem (1.1) into the Schrödinger equation

$$H_\epsilon \phi(z) = -\frac{d^2}{dz^2} \phi(z) + \left[z^2 + \frac{\tilde{\lambda}^2 - \frac{1}{4}}{z^2} - \tilde{\alpha} \right] \phi(z) = -\frac{1}{z^2} \tilde{E} (-iz)^{2\epsilon} \phi(z) \quad (6.1)$$

where

$$\tilde{M} = -1 + \frac{2}{M+1} = -1 + \epsilon, \quad \tilde{E} = \left(\frac{2}{M+1} \right)^{\frac{2M}{M+1}} E, \quad \tilde{\lambda} = \frac{2}{M+1} \lambda, \quad \tilde{\alpha} = \frac{2}{M+1} \alpha \quad (6.2)$$

and we have set $\epsilon = 2/(M+1)$. Under the duality transformation, the contour \mathcal{C} transforms into a curve equivalent to an M -independent straight line running just below the real axis.

The inhomogeneous complex square well of appendix D appears from (6.1) in the large- M (small ϵ) limit, when the right-hand side reduces to an additional angular momentum term so that (6.1) becomes the (\mathcal{PT} -symmetric) simple harmonic oscillator, when viewed as an eigenproblem for $\tilde{\alpha}$. The (unnormalised) eigenfunctions

$$\phi_n^\pm(z) = z^{\frac{1}{2} \pm \Lambda} e^{-\frac{z^2}{2}} L_n^{\pm \Lambda}(z^2), \quad \Lambda = \sqrt{\tilde{\lambda}^2 + \tilde{E}_n} \quad (6.3)$$

correspond to the $\tilde{\alpha}$ eigenvalues

$$\tilde{\alpha}_n^\pm = 4n + 2 \pm 2\sqrt{\tilde{\lambda}^2 + \tilde{E}_n}. \quad (6.4)$$

Alternatively the problem at $M = \infty$ can be considered at fixed $\tilde{\alpha}$ as a generalised eigenproblem for \tilde{E} , with the (entirely real) spectrum following on rearranging (6.4):

$$\tilde{E}_n = (2n + 1 - \frac{1}{2}\tilde{\alpha})^2 - \tilde{\lambda}^2, \quad n = 0, 1, \dots \quad (6.5)$$

The pair of levels \tilde{E}_n and \tilde{E}_m , $n \neq m$, will be degenerate whenever $\tilde{\alpha} = 2(n + m + 1)$. Thus degeneracies occur in the spectrum on the horizontal lines $\tilde{\alpha} = 4, 6, 8, \dots$ in the $(2\tilde{\lambda}, \tilde{\alpha})$ plane, and a perturbative treatment will be reliable close to these lines.

The eigenvalue problem at large but finite M can be explored by taking ϵ small and truncating the full Hamiltonian H_ϵ to the 2×2 subspace spanned by the eigenfunctions ϕ^\pm associated with the levels

$$\tilde{E}^+ = (q - 2p + \eta/2)^2 - \tilde{\lambda}^2, \quad \tilde{E}^- = (q - 2p - \eta/2)^2 - \tilde{\lambda}^2, \quad q \in \mathbb{Z}^+. \quad (6.6)$$

This pair of eigenvalues will be almost-degenerate when $\tilde{\alpha} = 2(q+1)+\eta$ and $p = 0, 1, \dots [(q-1)/2]$ provided η is small. When η is zero the eigenvalues merge to the single eigenvalue $E_0 := E_p^+ = E_{q-p}^-$. Since the eigenfunctions (6.3) satisfy the nonstandard eigenproblem

$$H_0\phi^\pm = -\frac{1}{z^2}\tilde{E}^\pm\phi^\pm, \quad (6.7)$$

the usual inner product must be weighted by a factor of z^{-2} , and so we define

$$(\phi_n|\phi_m) = \int_{\mathbb{R}-i\varepsilon} \phi_n(z)\phi_m(z)z^{-2}dz \quad (6.8)$$

with a small positive ε to avoid any singularities at $z = 0$. Using the integral (C.1) and analytic continuation as necessary, the orthonormal eigenfunctions are

$$\phi^+(z) = \frac{\sqrt{2p!(q-2p+\eta/2)}}{\sqrt{(1-e^{\pi i\eta})\Gamma(q-p+\eta/2+1)}} z^{1/2+q-2p+\eta/2} e^{-z^2/2} L_p^{q-2p+\eta/2}(z^2) \quad (6.9)$$

and

$$\phi^-(z) = \phi^+(z)|_{p \rightarrow q-p} = \frac{\sqrt{2(q-p)!(2p-q+\eta/2)}}{\sqrt{(1-e^{\pi i\eta})\Gamma(p+\eta/2+1)}} z^{1/2+2p-q+\eta/2} e^{-z^2/2} L_{q-p}^{2p-q+\eta/2}(z^2). \quad (6.10)$$

In the truncated basis any eigenfunction ϕ can be approximated as $\phi = \mu\phi^+ + \nu\phi^-$ for some constants μ and ν . Applying H_ϵ to ϕ , the corresponding approximate eigenvalue \tilde{E} must satisfy

$$\tilde{E}^+ \frac{\phi^+}{z^2} + \nu \tilde{E}^- \frac{\phi^-}{z^2} = \frac{1}{z^2} (-iz)^{2\epsilon} \tilde{E} (\mu\phi^+ + \nu\phi^-), \quad (6.11)$$

given that ϕ^\pm are eigenfunctions of the unperturbed Hamiltonian (6.7). Thus taking inner product of (6.11) with ϕ^\pm in turn, we obtain

$$\begin{pmatrix} \tilde{E}^+ & 0 \\ 0 & \tilde{E}^- \end{pmatrix} \begin{pmatrix} \mu \\ \nu \end{pmatrix} = \tilde{E} \begin{pmatrix} (\phi^+|(-iz)^{2\epsilon}|\phi^+) & (\phi^+|(-iz)^{2\epsilon}|\phi^-) \\ (\phi^-|(-iz)^{2\epsilon}|\phi^+) & (\phi^-|(-iz)^{2\epsilon}|\phi^-) \end{pmatrix} \begin{pmatrix} \mu \\ \nu \end{pmatrix}. \quad (6.12)$$

We use the integral (C.1) in appendix C to calculate the required exact matrix elements. To leading order in ϵ and η , the matrix elements $H_{ab} = (\phi^a|(-iz)^{2\epsilon}|\phi^b)$ are

$$\begin{aligned} H_{++} &\approx 1 + \frac{2\epsilon}{\eta} + \left(\psi(q-2p) + \psi(q-2p+1) - \psi(q-p+1) \right) \epsilon \\ &\quad + 2 \left(\psi(q-2p) + \psi(q-2p+1) - \psi(q-p+1) \right) \frac{\epsilon^2}{\eta}; \end{aligned} \quad (6.13)$$

$$\begin{aligned} H_{--} &\approx 1 - \frac{2\epsilon}{\eta} + \left(\psi(q-2p) + \psi(q-2p+1) - \psi(p+1) \right) \epsilon \\ &\quad - 2 \left(\psi(q-2p) + \psi(q-2p+1) - \psi(q-p+1) \right) \frac{\epsilon^2}{\eta}; \end{aligned} \quad (6.14)$$

$$\begin{aligned} H_{+-} &\approx i(-1)^q \left[-\frac{2\epsilon}{\eta} + \frac{1}{2} \left(\psi(q-p+1) - \psi(p+1) \right) \epsilon \right. \\ &\quad \left. + 2 \left(\psi(q-p+1) - \psi(q-2p) - \psi(q-2p+1) \right) \frac{\epsilon^2}{\eta} \right]. \end{aligned} \quad (6.15)$$

Diagonalising the RHS of (6.12), the approximate eigenvalues at $\epsilon = 2/(M + 1)$ and $\tilde{\alpha} = 2(q + 1) + \eta$ are

$$\begin{aligned} \tilde{E}_{\pm} &= E_0 + \left(\frac{E_0}{2} (\psi(q-p+1) + \psi(p+1) - 4\psi(q-2p+1)) - \frac{E_0}{q-2p} - 2(q-2p) \right) \epsilon \\ &\pm \left[-4(q-2p)E_0\epsilon + (q-2p)^2\eta^2 + (q-2p)(\psi(q-p+1) - \psi(p+1))E_0\epsilon\eta \right. \\ &\quad \left. + \left(2(q-2p)(4\psi(q-2p+1) - 3\psi(p+1) - \psi(q-p+1) + 4\psi(q-2p)) E_0 + 4(q-2p)^2 \right) \epsilon^2 \right]^{1/2} \end{aligned} \quad (6.16)$$

where $E_0 = (q - 2p)^2 - \tilde{\lambda}^2$. Just as for $M \approx 1$, the exceptional points can be located by finding where the argument of the square root in (6.16) vanishes. Figure 22 shows the resulting curves of exceptional points in the $(2\lambda, \tilde{\alpha})$ plane for $M = 250$, taking $q = 1 \dots 5$ and $p = 0 \dots [(q - 1)/2]$. The match with the results from a numerical solution to the full problem is excellent, and indeed even at $M = 30$ the truncation method gives a plot essentially indistinguishable from that shown earlier in figure 18.

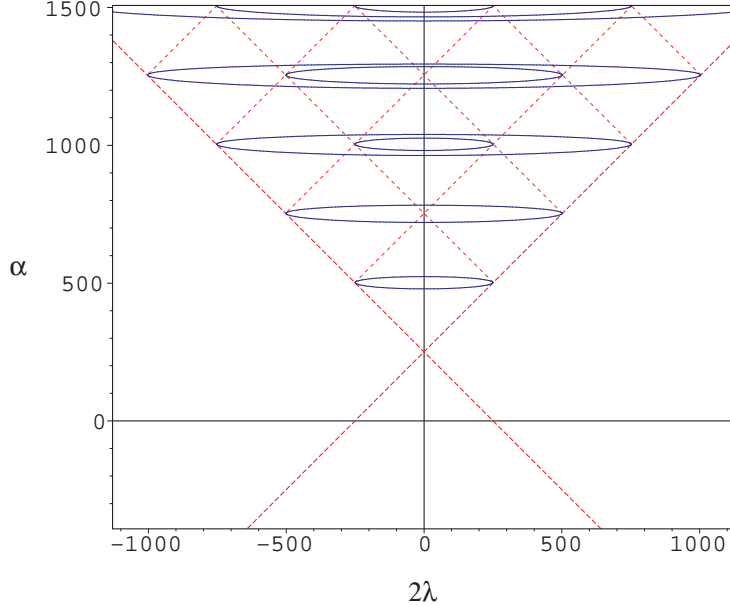


Figure 22: Perturbative predictions for the exceptional lines for $M = 250$.

The main features of the transitions are most clearly understood if only the terms proportional to η and ϵ/η are kept in the matrix elements H_{ab} . Rediagonalising (6.12), the approximate eigenvalues are

$$\tilde{E}_{\text{approx}} = E_0 \pm \sqrt{(q - 2p)^2\eta^2 - 4E_0(q - 2p)\epsilon} . \quad (6.17)$$

Demanding once again that the argument of the square root vanishes leads to the prediction that the exceptional points lie on the ellipses

$$4 \left(\frac{\alpha}{M+1} - q - 1 \right)^2 (q - 2p) - 4\epsilon \left((q - 2p)^2 - 4 \frac{\lambda^2}{(M+1)^2} \right) = 0 \quad (6.18)$$

in the $(2\lambda, \alpha)$ plane. Thus as M decreases from infinity isolated ellipses of unreality appear, starting from segments of the degenerate lines $\tilde{\alpha} = 4, 6, 8, \dots$ at $M = \infty$ and acquiring exactly the ‘nested’ structure seen in figures 18 and 22.

Table 3 compares the various levels of approximation used in this section with numerical data obtained from a direct treatment of the ordinary differential equation, in the same notation as table 2. The table shows the comparison for sample values of ϵ , $\tilde{\lambda}$ and η , for $p = 0$, $q = 1$ (i.e. $\tilde{\alpha} = 4 + \eta$) and for $p = 0$, $q = 2$ (i.e. $\tilde{\alpha} = 6 + \eta$).

$p = 0, q = 1$				
	$\epsilon = 0.001, \tilde{\lambda} = -1.2, \eta = 0.01$		$\epsilon = 0.001, \lambda = -1.2, \eta = 0.25$	
E_{exact}	-0.48512051	-0.3988914	-0.679527538	-0.17313365
E_{trunc}	-0.48511885	-0.3988926	-0.679526948	-0.17313370
E_{\pm}	-0.48514998	-0.3989179	-0.695319170	-0.18874878
E_{approx}	-0.48312771	-0.3968723	-0.693495562	-0.18650444
$p = 0, q = 2$				
	$\epsilon = 0.01, \tilde{\lambda} = -3, \eta = 0.01$		$\epsilon = 0.01, \tilde{\lambda} = -3, \eta = 0.25$	
E_{exact}	-5.59855357	-4.36272053	-5.72941123	-4.20419136
E_{trunc}	-5.59525382	-4.36529048	-5.72605257	-4.20649571
E_{\pm}	-5.60435172	-4.35836985	-5.75706543	-4.20565613
E_{approx}	-5.63277168	-4.36722832	-5.80622578	-4.19377423

Table 3: Comparison of the various approximation methods used in section 6.

7 Conclusions

In this paper we have continued the project initiated in [1, 2], and mapped out the phase diagram of a three-parameter family of \mathcal{PT} -symmetric eigenvalue problems related to the Perk-Schultz models. Special features have enabled us to make precise the Jordan block structures at a subset of the exceptional points, going beyond the finite-dimensional examples which were the subject of most previous work. We have also uncovered some novel properties of the Bender-Dunne polynomials. The resulting phase diagrams at fixed M , consisting of lines of quadratic exceptional points punctuated by triply-exceptional (cubic) cusps, generalise the previously-observed story at $M = 3$ in an appealing way, and the perturbative treatment about $M = 1$ has allowed us to understand the transition to infinitely-many complex eigenvalues which occurs as M decreases below 1 from a new perspective. The dualities that we have used were crucial in making a reliable numerical treatment of the problem, and may be of independent theoretical interest, especially given the roles that this set of models plays as possibly the simplest example of an ODE/IM correspondence.

Acknowledgements – We would like to thank Adam Millican-Slater for previous collaboration, and Carl Bender, Uwe Gunther, Deiter Heiss, Joey Oliver, Mark Sorrell and Farid Tari for useful conversations and help. PED, TCD and AL thank Torino University, and PED, TCD and RT thank APCTP, Pohang and the Galileo Galilei Institute, Florence, for hospitality at various stages of this project. PED was partially supported by the International Molecule program ‘Aspects of Quantum Integrability’, and thanks the Yukawa Institute for Theoretical Physics for its hospitality during this period. The project was also partially supported by INFN grants TO12 and PI11, NATO grant number PST.CLG.980424, STFC rolling grant ST/G000433/1, a Nuffield Foundation grant number NAL/32601, and a grant from the Leverhulme Trust.

A Basis for an $n \times n$ Jordan block

(See [16] for a discussion of the $n = 2$ case.) To illustrate a method we can use to construct the basis of an $n \times n$ Jordan block, which arises when n eigenstates merge, we will work with a toy model. Take an $n \times n$ matrix L , depending on one parameter ϵ :

$$L(\epsilon) = \begin{pmatrix} 0 & 1 & 0 & \dots \\ \vdots & \ddots & \ddots & 0 \\ 0 & \dots & 0 & 1 \\ \epsilon & 0 & \dots & 0 \end{pmatrix}. \quad (\text{A.1})$$

This has n independent eigenvectors:

$$\psi_j = \begin{pmatrix} 1 \\ e^{(2\pi i j/n)} \epsilon^{1/n} \\ e^{(4\pi i j/n)} \epsilon^{2/n} \\ \vdots \\ e^{2\pi(n-1)ij/n} \epsilon^{(n-1)/n} \end{pmatrix}, \quad j = 1 \dots n. \quad (\text{A.2})$$

When $\epsilon = 0$, $L(\epsilon)$ has a Jordan block form, but at this point all n eigenvectors ψ_j become equal and so no longer form a basis. We therefore need to construct a new basis consisting of the vectors $\phi^{(k)}$, $k = 0 \dots n - 1$ which satisfy a Jordan chain

$$L(\epsilon)\phi^{(0)} \Big|_{\epsilon=0} = 0 \quad (\text{A.3})$$

$$L(\epsilon)\phi^{(k)} \Big|_{\epsilon=0} = \phi^{(k-1)} \Big|_{\epsilon=0}, \quad k = 1 \dots n - 1. \quad (\text{A.4})$$

For simplicity we begin with the eigenvector ψ_n where

$$L(\epsilon)\psi_n(\epsilon) = \epsilon^{1/n}\psi_n(\epsilon). \quad (\text{A.5})$$

Clearly $\phi^{(0)} = \psi_n(\epsilon)$ satisfies the condition (A.3) when $\epsilon = 0$. We could choose $\phi^{(0)}$ to be any of the ψ_j here; each one would lead to a different normalisation for the $\phi^{(k)}$ below.

Before we construct the other basis vectors, we introduce some notation. Let

$$D \equiv n\epsilon^{\frac{n-1}{n}} \frac{d}{d\epsilon} \quad (\text{A.6})$$

and

$$\tilde{L} \equiv \frac{dL}{d\epsilon}. \quad (\text{A.7})$$

Note that L is linear in ϵ so $\frac{d\tilde{L}}{d\epsilon} = 0$. We now have the following commutation relations

$$[D, \epsilon^{k/n}] = k\epsilon^{(k-1)/n} \quad (\text{A.8})$$

$$[D, L] = n\epsilon^{(n-1)/n} \tilde{L} \quad (\text{A.9})$$

$$[D, \tilde{L}] = 0. \quad (\text{A.10})$$

Finally, define

$$\phi^{(k+1)} \equiv \frac{1}{k+1} D\phi^{(k)}. \quad (\text{A.11})$$

By induction, it is easy to show that acting with D on (A.5) k times for $1 \leq k \leq n - 1$ gives

$$\sum_{j=0}^{k-1} \prod_{i=0}^j \frac{(n-i)}{(j+1)!} \epsilon^{\frac{n-j-1}{n}} \tilde{L}\phi^{(k-j-1)} + L\phi^{(k)} = \phi^{(k-1)} + \epsilon^{\frac{1}{n}}\phi^{(k)}. \quad (\text{A.12})$$

When $\epsilon = 0$ this satisfies (A.4), so an appropriate basis is

$$\phi^{(0)} = \psi_n \quad (\text{A.13})$$

and

$$\phi^{(k)} = \frac{1}{k} D \phi^{(k-1)} \quad (\text{A.14})$$

for $k = 1 \dots n - 1$.

B Two dualities

As noted in [30], useful relations between spectral problems which arise in the ODE/IM correspondence can often be found by simple variable changes. Here, starting from (1.1) and setting $z = ix$ as in (2.14) to obtain

$$-\frac{d^2}{dz^2} \psi(z) + \left[z^{2M} + \alpha z^{M-1} + \frac{\lambda^2 - \frac{1}{4}}{z^2} + E \right] \psi(z) = 0 \quad (\text{B.1})$$

we exploit the fact that, for arbitrary β , the combined substitutions $z = y^\beta$, $\psi(z) = y^{(\beta-1)/2} \phi(y)$, transform $d^2\psi/dz^2$ without introducing a first derivative term:

$$\frac{d^2}{dz^2} \psi(z) = \frac{y^{3/2-3\beta/2}}{\beta^2} \left[\frac{d^2}{dy^2} - \frac{\beta^2 - 1}{4y^2} \right] \phi(y) \quad (\text{B.2})$$

so that the equation becomes

$$-\frac{d^2}{dy^2} \phi(y) + \beta^2 \left[y^{2(M+1)\beta-2} + \alpha y^{(M+1)\beta-2} + \frac{\beta^2 \lambda^2 - \frac{1}{4}}{\beta^2 y^2} + E y^{2\beta-2} \right] \phi(y) = 0. \quad (\text{B.3})$$

Two important special cases are $\beta = 1/(M+1)$ and $\beta = 2/(M+1)$.

1) $\beta = 1/(M+1)$: setting $y = \kappa w$ with $\kappa = ((M+1)/\sqrt{-E})^{M+1}$ leads to

$$-\frac{d^2}{dw^2} \phi(w) + \left[-w^{2\tilde{M}} + \tilde{\alpha} \sqrt{\tilde{E}} w^{-1} + \frac{\tilde{\lambda}^2 - \frac{1}{4}}{w^2} + \tilde{E} \right] \phi(w) = 0 \quad (\text{B.4})$$

where

$$\tilde{M} = -\frac{M}{M+1}, \quad \tilde{E} = \frac{(M+1)^{2M}}{(-E)^{M+1}}, \quad \tilde{\lambda} = \frac{1}{M+1} \lambda, \quad \tilde{\alpha} = \frac{1}{M+1} \alpha. \quad (\text{B.5})$$

This generalises the duality used in [30] to inhomogeneous potentials[§].

2) $\beta = 2/(M+1)$: setting $y = \kappa w$ with $\kappa = \sqrt{(M+1)/2}$ yields

$$-\frac{d^2}{dw^2} \phi(w) + \left[w^2 + \tilde{E} w^{2\tilde{M}} + \frac{\tilde{\lambda}^2 - \frac{1}{4}}{w^2} + \tilde{\alpha} \right] \phi(w) = 0 \quad (\text{B.6})$$

where

$$\tilde{M} = -1 + \frac{2}{M+1}, \quad \tilde{E} = \left(\frac{2}{M+1} \right)^{\frac{2M}{M+1}} E, \quad \tilde{\lambda} = \frac{2}{M+1} \lambda, \quad \tilde{\alpha} = \frac{2}{M+1} \alpha. \quad (\text{B.7})$$

To obtain an equivalence between eigenvalue problems, the transformation of the boundary conditions under the mappings must be tracked. The boundary conditions from section 1 translate into the requirement that eigenfunctions of the initial problem (B.1) should decay in $i\mathcal{S}_{-1}$

[§]It is interesting that, while [30] is indeed the first time that this duality was applied in the context of integrable quantum field theory, the homogeneous case can be traced back to (Isaac) Newton: see [31, 32].

and $i\mathcal{S}_1$, where the sectors \mathcal{S}_k were defined in (1.3). After the transformation the simultaneous decay should instead be in $i\tilde{\mathcal{S}}_{-1}$ and $i\tilde{\mathcal{S}}_1$, where for case **1**, Newton's duality,

$$\tilde{\mathcal{S}}_k = \{x \in \mathbb{C} : |\arg(ix) - \pi k| < \pi/2\}, \quad (\text{B.8})$$

while for case **2** ($\beta = 2/(M+1)$),

$$\tilde{\mathcal{S}}_k = \{x \in \mathbb{C} : |\arg(ix) - \pi k/2| < \pi/4\}. \quad (\text{B.9})$$

In both cases the transformed sectors are independent of M , reflecting the fact that the leading terms in (B.5) and (B.6) at large $|w|$, \tilde{E} and w^2 respectively, are themselves independent of M . For the first duality it might appear that the sectors $i\tilde{\mathcal{S}}_{\pm 1}$ coincide, but this is not so – the branch cut in the original problem (1.1) becomes a cut along the negative real axis of the w plane, and so the two sectors lie on top of each other on the full Riemann surface of the problem. For the second duality the sectors are those of the simple harmonic oscillator and this makes (B.6) particularly useful for numerical work: eigenvalues can be found by solving the ODE on a straight, M -independent contour, running vertically (parallel to the imaginary axis) in the right half of the complex w plane. An efficient approach uses WKB asymptotics at large $|w|$ as initial conditions for a pair of numerical solutions, ϕ_{-1} and ϕ_1 , decaying as $\Im m w \rightarrow \pm\infty$, and then locates the eigenvalues by looking for zeros of the Wronskian $W[\phi_{-1}, \phi_1]$, evaluated in the neighbourhood of the origin where both numerical solutions are reliable. This method was used to produce many of the figures in this paper.

Replacing w by w/i trivially rotates the dual problems back to a more usual ‘ \mathcal{PT} -symmetric’ form. The mappings can also be used to give equivalences for spectral problems initially specified by the simultaneous decay of eigenfunctions on more widely-separated pairs of Stokes sectors than \mathcal{S}_{-1} and \mathcal{S}_1 . The homogeneous cases of these problems were discussed in [27], and related to fused transfer matrices in integrable models in [11].

C Useful formulae

This appendix records a number of formulae used in the main text. All can be inferred from the following basic integral, involving a pair of Laguerre polynomials:

$$\begin{aligned} & \int_0^\infty t^\alpha t^{(\gamma+\rho)/2} e^{-t} L_m^\rho(t) L_n^\gamma(t) dt \\ &= \frac{(\frac{1}{2}(\gamma-\rho)-\alpha)_n (\rho+1)_m}{n! m!} \Gamma(\frac{1}{2}(\gamma+\rho)+1+\alpha) \times \\ & \quad {}_3F_2(-m, \frac{1}{2}(\rho+\gamma)+1+\alpha, \frac{1}{2}(\rho-\gamma)+1+\alpha; \rho+1, \frac{1}{2}(\rho-\gamma)+1+\alpha-n; 1) \\ &= \frac{\Gamma(\frac{1}{2}(\gamma+\rho)+1+\alpha)}{m! n!} \times \\ & \quad \sum_{k=0}^m \binom{m}{k} (\rho+1+k)_{m-k} (\frac{1}{2}(\rho+\gamma)+1+\alpha)_k (\frac{1}{2}(\rho-\gamma)+1+\alpha)_k (\frac{1}{2}(\gamma-\rho)-\alpha)_{n-k} \quad (\text{C.1}) \end{aligned}$$

where $(a)_n = a(a+1)\dots(a+n-1)$ is the Pochhammer symbol and ${}_3F_2$ is a generalised hypergeometric function. The first version of this result can be found in [29]; it generalises a formula for the case $\gamma = \rho$ that was given in [33]. The symmetry of the final expressions under the simultaneous exchanges $m \leftrightarrow n$, $\rho \leftrightarrow \gamma$ is not obvious, though it can be checked.

In section 5 the matrix elements $\langle \phi_n^\pm(x) | (ix)^{2M} | \phi_m^\pm(x) \rangle$ and $\langle \phi_n^\pm(x) | (ix)^{2M} | \phi_m^\mp(x) \rangle$ were needed for general M , where $\phi_n^+(x)$ and $\phi_n^-(x)$ are the normalised wavefunctions given by (5.7). The relevant calculations were also carried out by Millican-Slater in [29], and we reproduce his

final results here. The matrix element $\langle \phi_n^+ | (ix)^{2M} | \phi_m^+ \rangle$ is

$$\begin{aligned} \langle \phi_n^+ | (ix)^{2M} | \phi_m^+(x) \rangle = & \\ & (\cos(M\pi) + \sin(M\pi) \cot(\lambda\pi)) \frac{(-M)_n (\lambda+1)_m}{\sqrt{n!m! \Gamma(\lambda+m+1) \Gamma(\lambda+n+1)}} \times \\ & \Gamma(\lambda+M+1) {}_3F_2(-m, \lambda+M+1, 1+M; \lambda+1, 1+M-n; 1). \end{aligned} \quad (\text{C.2})$$

For $M = 1$ (one of the cases needed) there is a negative integer in one of the second group of entries of the hypergeometric function in (C.2), and so for certain values of n and m these functions may be undefined. This is the case when $n - 2 < m$. However, for $|n - m| \geq 2$ the symmetry of the inner products in n and m can be used to avoid the problem. In these cases, when $M = 1$, the $(-M)_n$ in the expressions above become $(-1)_n = 0$ so the inner products are zero. For $n = m$ and $n = m \pm 1$, by taking the limit $M \rightarrow 1$ in (C.2) it can be shown [29] that the only non-zero inner products are

$$\langle \phi_n^+(x) | x^2 | \phi_n^+(x) \rangle = 1 + \lambda + 2n \quad (\text{C.3})$$

$$\langle \phi_{n+1}^+(x) | x^2 | \phi_n^+(x) \rangle = \sqrt{\frac{n+1}{n+\lambda+1}} (\lambda - n). \quad (\text{C.4})$$

The matrix elements corresponding to (C.2), (C.3) and (C.4) for ϕ_n^- can be found by sending $\lambda \rightarrow -\lambda$.

The matrix element $\langle \phi_n^+(x) | (ix)^{2M} | \phi_m^-(x) \rangle$ is given by

$$\begin{aligned} \langle \phi_n^+(x) | (ix)^{2M} | \phi_m^-(x) \rangle = & i \frac{\sin(M\pi) (1-\lambda)_m (\lambda-M)_n \Gamma(M+1)}{|\sin(\pi\lambda)| \sqrt{\Gamma(1-\lambda+m) \Gamma(1+\lambda+n) m! n!}} \\ & \times {}_3F_2(-m, 1+M, M+1-\lambda; 1-\lambda, M+1-\lambda-n; 1), \end{aligned} \quad (\text{C.5})$$

which, unlike (C.2), is always well defined at $M = 1$.

D The inhomogeneous complex square well

In the main text, the large- M limit of the spectrum of

$$\left[-\frac{d^2}{dx^2} - (ix)^{2M} - \alpha (ix)^{M-1} + \frac{\lambda^2 - \frac{1}{4}}{x^2} \right] \psi(x) = E \psi(x), \quad \psi(x) \in L^2(\mathcal{C}), \quad (\text{D.1})$$

was needed. The $\alpha = 0, \lambda = 1/2$ case was investigated in [34], where it was dubbed the ‘complex square well’. To treat the more general case, we start with the same variable change as in [34], and set

$$x = \left(-i + \frac{z\pi}{2M} \right) E^{\frac{1}{2M}}. \quad (\text{D.2})$$

Taking the limit $M \rightarrow \infty$, using the identity $\lim_{M \rightarrow \infty} (1 + x/M)^M = e^x$ and dropping all subleading terms, (D.1) becomes

$$\left[\frac{d^2}{dz^2} + \frac{\pi^2}{16} \tilde{E} (1 + e^{i\pi z}) + \frac{\pi^2}{16} \sqrt{E} \tilde{\alpha} e^{i\pi z/2} + \frac{\pi^2}{16} \tilde{\lambda}^2 \right] \psi(z) = 0 \quad (\text{D.3})$$

where

$$\tilde{E} = \left(\frac{2}{M+1} \right)^2 E \quad (\text{D.4})$$

and the scaled parameters

$$\tilde{\lambda} = \frac{2\lambda}{M+1}, \quad \tilde{\alpha} = \frac{2\alpha}{M+1} \quad (\text{D.5})$$

were used to ensure the survival of the inhomogeneous and angular-momentum terms in the limit. Notice that in terms of $\tilde{\lambda}$ and $\tilde{\alpha}$, the parameters α_{\pm} of (2.1) are simply

$$\alpha_{\pm} = \frac{1}{4} (\tilde{\alpha} - 1 \pm 2\tilde{\lambda}). \quad (\text{D.6})$$

The special feature of this limit is that the resulting ODE (D.3) is exactly solvable. Here we highlight the link with the simple harmonic oscillator by making a further variable change to $w = \tilde{E}^{1/4} e^{i\pi z/4}$ and trading $\psi(w)$ for $\phi(w) = \sqrt{w} \psi(w)$. Substituting in, $\phi(w)$ satisfies

$$-\frac{d^2\phi}{dw^2} + \left[w^2 + \frac{\tilde{E} + \tilde{\lambda}^2 - \frac{1}{4}}{w^2} \right] \phi = -\tilde{\alpha} \phi. \quad (\text{D.7})$$

Boundary conditions should be imposed on the asymptotic Stokes lines $z = \pm 2 - iy$, $y \rightarrow \infty$ [34], which translate into the positive and negative imaginary axes in the complex w plane. That said, the spectrum of (D.7) can be recognised as that of the \mathcal{PT} -symmetric simple harmonic oscillator [11, 26], with ‘energy’ $\tilde{\alpha}$ and ‘angular momentum’ $-1/2 \pm \sqrt{\tilde{E} + \tilde{\lambda}^2}$ (the reversed sign of the energy is a result of the rotated quantisation contour for (D.7) compared to that used in [11]). Hence, from [11], (D.7) has a wavefunction normalisable on the quantisation contour if and only if

$$\tilde{\alpha} = 4n + 2 \pm 2\sqrt{\tilde{E} + \tilde{\lambda}^2}, \quad n = 0, 1, \dots \quad (\text{D.8})$$

which translates into our main result for the exact spectrum of (D.1) in the $M \rightarrow \infty$ limit:

$$\tilde{E}_n = (2n + 1 - \frac{1}{2}\tilde{\alpha})^2 - \tilde{\lambda}^2, \quad n = 0, 1, \dots \quad (\text{D.9})$$

Via $\tilde{E}_n = 4E_n/(M+1)^2$, this result also gives the leading behaviour of the original levels E_n as the limit is taken. For $\tilde{\lambda} = \tilde{\alpha} = 0$, this reproduces the result of [34]. Notice that the spectrum is entirely real for all values of $\tilde{\lambda}$ and $\tilde{\alpha}$, matching the situation at $M = 1$, the other exactly-solvable point.

References

- [1] P. Dorey, C. Dunning and R. Tateo, ‘Spectral equivalences, Bethe Ansatz equations, and reality properties in \mathcal{PT} -symmetric quantum mechanics’, *J. Phys. A* **34** (2001) 5679 [arXiv:quant-th/0103051].
- [2] P. Dorey, C. Dunning and R. Tateo, ‘Supersymmetry and the spontaneous breakdown of \mathcal{PT} symmetry’, *J. Phys. A* **34** (2001) L391 [arXiv:hep-th/0104119].
- [3] C.M. Bender and S. Boettcher, ‘Real spectra in non-hermitian Hamiltonians having \mathcal{PT} symmetry’, *Phys. Rev. Lett.* **80** (1998) 4243 [arXiv:physics/9712001].
- [4] P.F. Hsieh and Y. Sibuya, ‘On the asymptotic integration of second order linear ordinary differential equations with polynomial coefficients’, *J. Math. Anal. Appl.* **16** (1966) 84.
- [5] Y. Sibuya, *Global theory of a second-order linear ordinary differential equation with polynomial coefficient*, (Amsterdam: North-Holland 1975).
- [6] Y. Sibuya, ‘A boundary value problem in the complex plane’, in *Analytic Theory of Differential Equations*, Lecture Notes in Mathematics 183 (Springer-Verlag).
- [7] P. Dorey and R. Tateo, ‘Anharmonic oscillators, the thermodynamic Bethe ansatz and nonlinear integral equations’, *J. Phys. A* **32** (1999) L419 [arXiv:hep-th/9812211].
- [8] P. Dorey, C. Dunning and R. Tateo, ‘The ODE/IM correspondence’, *J. Phys. A* **40** (2007) R205 [arXiv:hep-th/0703066].

- [9] J.H.H. Perk and C.L. Schultz, ‘New families of commuting transfer matrices in q-state vertex models’, *Phys. Lett. A* **84** (1981) 407.
- [10] J. Suzuki, ‘Functional relations in Stokes multipliers - Fun with $x^6 + \alpha x^2$ potential’, *J. Statist. Phys.* **102** (2001) 1029 [arXiv:quant-ph/0003066].
- [11] P. Dorey and R. Tateo, ‘On the relation between Stokes multipliers and the T-Q systems of conformal field theory’, *Nucl. Phys. B* **563** (1999) 573 [arXiv:hep-th/9906219].
- [12] M. Sorrell, ‘Complex WKB analysis of a PT symmetric eigenvalue problem’, *J. Phys. A* **40** (2007) 10319 [arXiv:math-ph/0703030].
- [13] H. Aoyama, M. Sato and T. Tanaka, ‘General forms of a \mathcal{N} -fold supersymmetric family’, *Phys. Lett. B* **503** (2001) 423 [arXiv:quant-ph/0012065].
- [14] T. Kato, *Perturbation theory of linear operators* (Springer, Berlin, 1966).
- [15] W.D. Heiss, ‘Exceptional points of non-Hermitian operators’, *J. Phys. A* **37** (2004) 1 [arXiv:quant-ph/0304152].
- [16] A.V. Sokolov, A.A. Andrianov and F. Cannata, ‘Non-Hermitian quantum mechanics of non-diagonalizable Hamiltonians: puzzles with self-orthogonal states’, *J. Phys. A* **39** (2006) 10207 [arXiv:quant-ph/0602207].
- [17] U. Guenther, I. Rotter and B.F. Samsonov, ‘Projective Hilbert space structures at exceptional points’, *J. Phys. A* **40** (2007) 8815 [math-ph, arXiv:0704.1291v3].
- [18] N. Moiseyev, P.R. Certain and F. Weinhold, ‘Resonance properties of complex-rotated Hamiltonians’, *Mol. Phys.* **36** (1978) 1613;
N. Moiseyev, ‘Quantum theory of resonances: calculating energies, widths and cross-sections by complex scaling’, *Phys. Rep.* **302** (1998) 211.
- [19] D.T. Trinh, ‘Remarks on PT-norm in PT-symmetric quantum mechanics’, *J. Phys. A* **38** (2005) 3665 [arXiv:math-ph/0502009].
- [20] A.V. Turbiner, ‘Quasireactly solvable problems and SL(2) group’, *Commun. Math. Phys.* **118** (1988) 467.
- [21] C.M. Bender and G.V. Dunne, ‘Quasi-exactly solvable systems and orthogonal polynomials’, *J. Math. Phys.* **37** (1996) 6 [arXiv:hep-th/9511138].
- [22] C.M. Bender and M. Monou, ‘New quasi-exactly solvable sextic polynomial potentials’, *J. Phys. A* **38** (2005) 2179 [arXiv:quant-ph/0501053].
- [23] T. Curtright and L. Mezincescu, ‘Biorthogonal quantum systems’, *J. Math. Phys.* **48** (2007) 092106 [arXiv:quant-ph/0507015].
- [24] H. Whitney, ‘On singularities of mappings of Euclidean spaces. I. Mappings of the plane into the plane’, *Ann. Math.* **62** (1955) 374.
- [25] J.W. Bruce, ‘Motion pictures: an application of singularity theory’, *J. London Math. Soc.* (2), **30** (1984) 160;
J.W. Bruce, ‘Seeing – the mathematical viewpoint’, *The Mathematical Intelligencer* **6** (1984) 18.
- [26] M. Znojil, ‘ \mathcal{PT} -symmetric harmonic oscillators’, *Phys. Lett. A* **259** (1999) 220 [arXiv:quant-ph/9905020].
- [27] C.M. Bender, S. Boettcher and P. Meisinger, ‘PT-symmetric quantum mechanics’, *J. Math. Phys.* **40** (1999) 2201 [arXiv:quant-ph/9809072].
- [28] P. Dorey, A. Millican-Slater and R. Tateo, ‘Beyond the WKB approximation in PT-symmetric quantum mechanics’, *J. Phys. A* **38** (2005) 1305 [arXiv:hep-th/0410013].

- [29] A. Millican-Slater, *Aspects of PT -symmetric quantum mechanics*, Durham Ph.D. Thesis 2004.
- [30] V.V. Bazhanov, S.L. Lukyanov and A.B. Zamolodchikov, ‘Spectral determinants for Schroedinger equation and Q-operators of conformal field theory’, *J. Statist. Phys.* **102** (2001) 567 [arXiv:hep-th/9812247].
- [31] C. Quigg, ‘Realizing the potential of quarkonium’, in: *Chicago 1997, Twenty beautiful years of bottom physics*, 173 [arXiv:hep-ph/9707493].
- [32] A.K. Grant and J.L. Rosner, ‘Classical orbits in power law potentials’, *Am. J. Phys.* **62** (1994) 310.
- [33] N. Saad and R.L. Hall, ‘Integrals containing confluent hypergeometric functions with applications to perturbed singular potentials’, *J. Phys. A* **36** (2003) 7771.
- [34] C.M. Bender, S. Boettcher, H.F. Jones and V.M. Savage, ‘Complex square well — a new exactly solvable quantum mechanical model’, *J. Phys. A* **32** (1999) 6771 [arXiv:quant-ph/9906057].